Elsevier Editorial System(tm) for Chemical Geology
Manuscript Draft

Manuscript Number:

Title: Subduction Zone Metamorphic Pathway for Deep Carbon Cycling: II. Evidence from HP/UHP Metabasaltic Rocks and Ophicarbonates

Article Type: Research Article

Keywords: subduction; carbon cycle; decarbonation; arc volcanoes; stable isotopes

Corresponding Author: Dr. Gray Bebout, Ph.D.

Corresponding Author's Institution: Lehigh University

First Author: Nathan C Collins

Order of Authors: Nathan C Collins; Gray Bebout, Ph.D.; Samuel Angiboust, Ph.D.; Philippe Agard, Ph.D.; Marco Scambelluri, Ph.D.; Laura Crispini, Ph.D.; Timm John, Ph.D.

Published in Chemical Geology on 16 July 2015 Volume 412 (2015) 132–150

http://dx.doi.org/10.1016/j.chemgeo.2015.06.012

Abstract: Exposures of low-grade metabasalts and ophicarbonates in the Northern Apennines, and their high- and ultrahigh-pressure metamorphic equivalents in the Western and Ligurian Alps and Tianshan (representing an overall peak P-T range of 0.2-2.5 GPa, 250-610°C), allow investigation of the effects of prograde metamorphic devolatilization, and other fluid-rock interactions, on degrees of retention and isotopic evolution of C in subducting oceanic crust and associated mantle rocks. Such work can inform models of C cycling at convergent margins, helping constrain the efficiency of return of initially subducted C via arc volcanism and the fraction of this subducted C entering the deeper mantle beyond arcs.

In the metabasaltic rocks, the preservation of finely disseminated carbonate with δ13C overlapping that of seafloor-altered protoliths, and the minimal mineralogical evidence of decarbonation, indicate large degrees of carbonate retention in this suite extending to UHP conditions similar to those beneath modern volcanic fronts. For many of the metabasalts, the δ18O of this carbonate can be explained by closed-system equilibration with silicate phases (e.g., garnet, clinopyroxene) during HP/UHP metamorphism. Larger volumes of carbonate preserved in interpillow regions and as breccia-filling largely escaped decarbonation, showing little or no evidence for reaction with adjacent metabasalt. Calculated devolatilization histories demonstrate that, in a closed-system model, carbonate in metabasaltic rocks can largely be preserved to depths approaching those beneath volcanic fronts (80-90 km). Modeling of open-system behavior indicates that episodic infiltration of such rocks by H2O-rich fluids greatly enhances decarbonation. Trends in O-C isotope composition of carbonate in some metabasaltic suites likely reflect combined effects of infiltration by externally-derived fluid and some resulting decarbonation. Carbonated ultramafic rocks similarly show little mineralogical evidence for decarbonation, consistent with calculated reaction histories, and have δ13C largely overlapping with that of seafloor equivalents. However, the high-grade ophicarbonates show more restricted ranges in δ18O consistent with some control by infiltrating fluids, perhaps during subduction.

This combination of field, petrographic, and isotopic evidence, together with the calculated decarbonation histories, is consistent with minimal (likely <20%) loss of CO2 from these rocks during forearc metamorphism. Combining our results with those of Cook-Kollars et al. (2014; Chemical Geology) for associated W. Alps metasedimentary rocks, we suggest that the majority of the CO2

(perhaps as much as 80%, considering the full range of rock types) could be preserved in more intact volumes of subducting sediment, basalt, and ophicarbonate experiencing closed- or limited open-system conditions. In deep forearcs and beneath arcs, decarbonation, and also carbonate dissolution, could be enhanced in shear zones and highly fractured volumes experiencing larger fluid flux, and the amount of C loss by these mechanisms could be significant along disrupted subduction interfaces at which disparate lithologies are juxtaposed. Degrees of C loss by decarbonation, carbonate dissolution, and partial melting should be particularly significant as the subducting sections experience the greater heating related to exposure to the convecting mantle wedge (at depths of 80-120 km).

Research Highlights:

- Effects of subduction zone metamorphism on C cycling were examined.

- Calculated decarbonation history matches observed reaction history.

- Subducting metabasalts and ophicarbonates retain most of their C to 90 km depths.

- Metabasalts largely retain seafloor-inherited carbonate C isotope compositions.

- Extent of CO_2 retention depends upon degrees of infiltration by H_2O-rich fluids.

Subduction Zone Metamorphic Pathway for Deep Carbon Cycling: II. Evidence from HP/UHP Metabasaltic Rocks and Ophicarbonates

Nathan C. Collins[1], Gray E. Bebout[1], Samuel Angiboust[2], Philippe Agard[3], Marco Scambelluri[4], Laura Crispini[4], Timm John[5]

Published in Chemical Geology on 16 July 2015 Volume 412 (2015) 132–150
http://dx.doi.org/10.1016/j.chemgeo.2015.06.012

[1]Department of Earth and Environmental Sciences, Lehigh University, Bethlehem, Pennsylvania, 18015, U.S.A. (corresponding author; telephone: 610-758-5831; FAX: 610-758-3677; e-mail: geb0@lehigh.edu)

[2]GeoForschungsZentrum (GFZ), Telegrafenberg, D-14473 Potsdam, Germany

[3]ISTEP, Université Paris 06-UPMC, UMR CNRS 7193, 4 place Jussieu, F-75005, Paris, France

[4]Dip.Te.Ris Università degli Studi di Genova Via Balbi, 5 - 16126 Genova, Italy

[5]Institut für Geologische Wissenschaften, Malteserstrasse 74-100, D-12249 Berlin, Germany

submitted to *Chemical Geology* (2-09-15)

Abstract

Exposures of low-grade metabasalts and ophicarbonates in the Northern Apennines, and their high- and ultrahigh-pressure metamorphic equivalents in the Western and Ligurian Alps and Tianshan (representing an overall peak *P-T* range of 0.2-2.5 GPa, 250-610°C), allow investigation of the effects of prograde metamorphic devolatilization, and other fluid-rock interactions, on degrees of retention and isotopic evolution of C in subducting oceanic crust and associated mantle rocks. Such work can inform models of C cycling at convergent margins, helping constrain the efficiency of return of initially subducted C via arc volcanism and the fraction of this subducted C entering the deeper mantle beyond arcs.

In the metabasaltic rocks, the preservation of finely disseminated carbonate with $\delta^{13}C$ overlapping that of seafloor-altered protoliths, and the minimal mineralogical evidence of decarbonation, indicate large degrees of carbonate retention in this suite extending to UHP conditions similar to those beneath modern volcanic fronts. For many of the metabasalts, the $\delta^{18}O$ of this carbonate can be explained by closed-system equilibration with silicate phases (e.g., garnet, clinopyroxene) during HP/UHP metamorphism. Larger volumes of carbonate preserved in interpillow regions and as breccia-filling largely escaped decarbonation, showing little or no evidence for reaction with adjacent metabasalt. Calculated devolatilization histories demonstrate that, in a closed-system model, carbonate in metabasaltic rocks can largely be preserved to depths approaching those beneath volcanic fronts (80-90 km). Modeling of open-system behavior indicates that episodic infiltration of such rocks by H_2O-rich fluids greatly enhances decarbonation. Trends in O-C isotope composition of carbonate in some metabasaltic suites likely reflect combined effects of infiltration by externally-derived fluid and some resulting decarbonation. Carbonated ultramafic rocks similarly show little mineralogical evidence for decarbonation, consistent with calculated reaction histories, and have $\delta^{13}C$ largely overlapping with that of seafloor equivalents. However, the high-grade ophicarbonates show more restricted ranges in $\delta^{18}O$ consistent with some control by infiltrating fluids, perhaps during subduction.

This combination of field, petrographic, and isotopic evidence, together with the calculated decarbonation histories, is consistent with minimal (likely <20%) loss of CO_2 from these rocks during forearc metamorphism. Combining our results with those of Cook-Kollars et al. (2014; *Chemical Geology*) for associated W. Alps metasedimentary rocks, we suggest that the majority of the CO_2 (perhaps 80-90%, considering the full range of rock types) could be preserved in

more intact volumes of subducting sediment, basalt, and ophicarbonate experiencing closed- or limited open-system conditions. In deep forearcs and beneath arcs, decarbonation, and also carbonate dissolution, could be enhanced in shear zones and highly fractured volumes experiencing larger fluid flux, and the amount of C loss by these mechanisms could be significant along disrupted subduction interfaces at which disparate lithologies are juxtaposed. Degrees of C loss by decarbonation, carbonate dissolution, and partial melting should be particularly significant as the subducting sections experience the greater heating related to exposure to the convecting mantle wedge (at depths of 80-120 km).

1. Introduction

Understanding of deep-Earth C flux in subducting oceanic lithosphere and sediments is crucial to modeling volatiles contributions to volcanic arcs, evolution of the atmosphere, and long-term degassing or regassing of the mantle (Berner et al., 1983; Berner, 1999; Zhang and Zindler, 1993; Marty and Toltskhin, 1998; Dasgupta and Hirschmann, 2010; Van Der Meer et al., 2014). Current understanding of the degrees of C retention to great depths in subduction zones is largely based on studies of volcanic gas output in comparison with subduction zone inputs, the latter based on knowledge of seafloor lithologies (see Hilton et al., 2002). Additional understanding has come from theoretical and experimental studies of phase stabilities in subducting oceanic lithologies (e.g., Kerrick and Connolly, 1998, 2001a,b; Molina and Poli, 2000; Gorman et al., 2006; Poli et al., 2009; Tsuno and Dasgupta, 2011; Schmidt and Poli, 2014; Cook-Kollars et al., 2014). There is general agreement that the behavior of C (and other major volatiles) along the subduction-zone metamorphic pathway must be taken into account when assessing long-term Earth degassing and atmosphere evolution (Bebout, 1995, 2007b, 2014; Javoy, 1998; Kerrick, 2001; Dasgupta and Hirschmann, 2010; Dasgupta, 2013; Cook-Kollars et al., 2014). However, there has been relatively little petrologic and geochemical study of decarbonation, and other mechanisms of C mobilization, in high-pressure (HP) and ultrahigh-

97 pressure (UHP) metamorphic suites directly representing the pathway taken by appropriate rock
98 types subducting through forearcs and to beneath arcs.
99 A number of studies have considered global C subduction flux through comparison of
100 subduction zone inputs in sediments, altered oceanic crust, and hydrated ultramafic rocks and
101 subduction outputs in volcanic gases (e.g. Bebout 1995, 2007b, 2014; Hilton et al., 2002; Jarrard,
102 2003; Dasgupta and Hirschmann, 2010; Dasgupta, 2013). The complexity and related uncertainty
103 of these estimates are evident in the large ranges of published input flux estimates presented in
104 **Table 1** (also see Cook-Kollars et al., 2014). The combination of the uncertainties in the inputs
105 and outputs results in a wide range in the estimates of volcanic arc return efficiency (16 - 80%
106 arc return of the C entering trenches; **Table 1**). Some studies of arc volcanic CO_2 emissions have
107 estimated the efficiencies of volcanic return of deeply subducted C for individual margins (e.g.,
108 Hilton et al., 2002; Shaw et al., 2003; Zimmer et al., 2004; de Leeuw et al., 2007; Marin-Ceron et
109 al., 2010; Halldorsson et al., 2013). To examine the sourcing of C flux measured in volcanic
110 gases, de Leeuw et al. (2007) compared C inputs measured by Li and Bebout (2005) for
111 sediments outboard of the Central America trench. They suggested that contributions of
112 sedimentary C alone could account for the measured output of gases and estimated a C return of
113 12-18% in Costa Rica and ~29% in El Salvador. The lack of a contribution of volatiles from
114 subducting oceanic crust to arc volcanic gases has also been suggested by Sano et al. (2001),
115 Hilton et al. (2002), and Zimmer et al. (2004). However, it could be difficult to distinguish the
116 contributions of CO_2 from carbonate sediment and from carbonate in altered oceanic crust based
117 on the $CO_2/^3He$ and $\delta^{13}C$ of the volcanic gases (see House et al., 2014).
118 Theoretical studies have calculated phase stabilities for sediments, oceanic crust, and
119 ultramafic lithologies associated with inputs into subduction zones (Molina and Poli, 2000;

Kerrick and Connolly, 1998, 2001a,b; Wei and Powell, 2003; Wei et al., 2003; Proyer, 2003; Connolly, 2005; Gorman et al., 2006; Cook-Kollars et al., 2014). Connolly (2005) calculated mineral assemblages and volatiles concentrations for a wide range of sediment compositions, along subduction-zone *P-T* paths for modern margins, and suggested a closed-system model where decarbonation in subducting sediments allows CO_2 to be expelled from sediments without the influence of externally-derived H_2O fluids. In contrast, Gorman et al. (2006) investigated "open" system behavior in which crustal material, and sub-crustal slab ultramafic rocks, can contribute H_2O-rich fluids to overlying sediments and basalts, thus driving decarbonation reactions. The coupling of external fluid-ingress and decarbonation within subducting slabs has been described in some studies of HP rocks (e.g., John et al., 2008; Ague and Nicolescu, 2014), and the opposite has also been described, with carbonation occurring along major intra-slab fluid conduits (Beinlich et al., 2010; John et al., 2012). Closed- and open-system scenarios can produce drastically differing degrees of forearc devolatilization (see Gorman et al., 2006; discussion by Cook-Kollars et al., 2014), pointing to the need for "ground-truthing" by detailed study of devolatilization and fluid mobility in exposures of HP/UHP-metamorphosed oceanic lithologies.

Few studies have investigated the degrees of deep retention of C, as carbonate or reduced C (the latter largely metamorphosed organic matter), in appropriate lithologies (sediment, oceanic crust, and carbonated ultramafic rocks) and over the wide range of *P-T* conditions representative of trench to subarc metamorphism in subduction zones. The studies to date, mostly focusing on metasedimentary suites, have indicated substantial retention of C and other volatiles during the relatively cool metamorphic conditions experienced at <40 km depths in most forearcs (see Bebout, 1995; Bebout and Fogel, 1992; Sadofsky and Bebout, 2003) and extending to depths

143 approaching those beneath volcanic fronts (e.g., in the HP/UHP units in the Italian Alps; Cook-
144 Kollars et al., 2014; also see Busigny et al., 2003; Bebout et al., 2013). Greater degrees of
145 devolatilization and associated volatiles losses, including C isotope shifts in reduced C, occur in
146 metasedimentary rocks along relatively warm subduction-zone *P-T* paths, such as those
147 represented by the higher-grade units of the Catalina Schist (see Bebout, 1991a, 1995; Bebout
148 and Fogel, 1992). Other field and petrologic studies provide descriptions for UHP carbonate
149 rocks at individual localities without detailed work evaluating extents of decarbonation and
150 related isotopic shifts (e.g. Becker and Altherr, 1992; Kato et al., 1997; Zheng et al., 2003;
151 Castelli et al., 2007; van der Straaten et al., 2008, 2012; Proyer et al., 2014; Lu et al., 2014). The
152 smaller number of studies of HP/UHP metabasaltic rocks conducted at single localities, or over
153 small ranges in grade (prehnite-pumpellyite to blueschist facies), have similarly indicated
154 retention of C in subducting oceanic crust, with little or no isotopic shift, across metamorphic
155 grades (Cartwright and Barnicoat, 1999, 2003; Miller et al., 2001). This points to the need for
156 more thorough study of C loss from altered oceanic crust (AOC) and ultramafic rocks, the latter
157 representing either peridotite hydrated and carbonated on the seafloor or sub-crustal slab
158 ultramafic rocks hydrated and carbonated during slab bending and associated faulting and deep
159 infiltration by seawater (see discussion of faulting and infiltration process by Ranero et al., 2005).
160 The deep decarbonation, and overall C loss history, of deeply subducting AOC is particularly
161 key to understanding subduction C cycling as this lithology could convey one-half to two-thirds
162 of the subduction C input inventory into trenches (**Table 1**; see Dasgupta and Hirschmann, 2010;
163 Dasgupta, 2013; Cook-Kollars et al., 2014). The C subduction input in carbonated ultramafic
164 rocks is likely far smaller, but still a significant flux (see Alt et al., 2013; **Table 1**).

In this study, we investigated the effects of prograde metamorphism, devolatilization, and other fluid-rock interactions on the retention and isotopic evolution of C in AOC and hydrated and carbonated ultramafic rocks that experienced HP/UHP metamorphism over a wide range of estimated peak temperatures and pressures (250-625°C, 0.3-2.9 GPa). The work focused mostly on exposures in the Italian (and French) Alps, the Ligurian Alps, and the northern Apennines containing intact ophiolitic sequences and related cover sediments that experienced widely varying degrees of HP/UHP metamorphism (see **Fig. 1A**; geographic coordinates for these exposures are provided in **Supplementary Table 1**). The rocks in the Western Alps are known to have experienced smaller amounts of exhumation-related overprinting than exposures of similar rocks in the Eastern and Central Alps and in most other HP/UHP metamorphic terrains around the world (Platt, 1986; Desmons et al., 1999a,b; Jolivet et al., 2003; Zheng, 2012), affording a more thorough assessment of prograde metamorphic devolatilization history (see Bebout, 2007a; Bebout et al., 2013). In this paper, we provide a smaller dataset for carbonate in veins, and as finely disseminated carbonate, in well-studied eclogites in the Tianshan, including eclogites sampled across the envelopes of veins interpreted to be significant intraslab fluid conduits and eclogites that were rehydrated to blueschist along the plate interface during their exhumation (Zack and John, 2007; van der Straaten et al., 2008, 2012; Beinlich et al., 2010; John et al., 2012). We integrate field and petrologic observations, theoretical calculations of devolatilization history (using the Perple_X software; Connolly, 2005), and O and C isotope data for these rocks, largely focusing on carbonate (and decarbonation history) but with some attention paid to the minor reduced C that could reside in the metabasalts. A companion paper (Cook-Kollars et al., 2014) examined the record of devolatilization, and C release and mobility,

187 in the metasedimentary rocks exposed at most of the localities in the Italian and French Alps
188 investigated in our study (Cottian Alps and at Lago di Cignana).
189
190 **2. Geologic Setting**
191 The NW Italian and French Alps contain an abundance of Jurassic ophiolitic fragments that
192 were formed ~160-170 Ma in the paleo-Tethys Ocean and rapidly subducted (~3 to 5 Ma) to
193 peak metamorphic conditions ~45 Ma (Gebauer et al., 1997; Rubatto and Hermann, 2001, 2003).
194 This region is of particular interest as it preserves slices of intact ophiolitic sequences
195 metamorphosed over a wide range of peak *P-T* conditions (see **Fig. 1**), showing relatively small
196 degrees of retrogression due to exhumation (Rubatto and Hermann, 2001; Parrish et al., 2006)
197 and lithologically resembling modern Atlantic-type (slow-spreading rate) oceanic lithosphere
198 (Lagabrielle and Cannat, 1990; Tricart and Lemoine, 1991; Cannat et al., 1997).
199 **Internal Ligurides, Sestri Voltaggio Zone and Voltri Massif, Italy.** Several units in the
200 Internal Liguride units of the Northern Apennines, and of the blueschist to eclogite facies Sestri
201 Voltaggio Zone and Voltri Massif, were sampled due to their exposure of ophiolitic sequences
202 ranging from low-grade to HP conditions. Peak *P-T* conditions extend from 160-210°C at 0.2-0.3
203 GPa in the Bracco unit (Internal Liguride), 270-310°C at 0.6 GPa in the Mt. Figogna unit, and
204 300-350°C at 0.7 GPa in the Cravasco-Voltaggio unit (Leoni, et al., 1996), to ~550˚C at 2.0-2.5
205 GPa in Voltri. Several studies have investigated the fluid mobility and redistribution during the
206 closed system retrogression of the high-pressure Voltri Massif (e.g., Vallis and Scambelluri,
207 1996; Scambelluri et al., 2004, 2007).
208 **Ubaye Valley, France.** Exposures at Pic du Pelvat in the Ubaye Valley, France, include
209 ophicarbonates and relatively undeformed pillow basalts, with intact interstitial material. This

crustal sequence is overlain by radiolarian chert and carbonate rocks (Tricart and Lemoine, 1986) and all rocks have experienced peak *P-T* conditions of 325-375°C and 1.1-1.4 GPa (Michard et al., 2004). This ophiolite fragment (with aerial exposure of about 1.5 km^2) was described by Tricart and Lemoine (1986) as an isolated megaboudin (slab) of oceanic crust retaining its original contact with the highly deformed Schistes Lustres metasedimentary section.

Monviso, Italy. The two tectonic slices of the Monviso ophiolite preserve eclogite-facies metamorphism at 480-515°C at 2.1 ± 0.3 GPa in the Monviso Unit and 524 to 571°C at 2.5 to 2.8 GPa in the Lago Superiore Unit (Angiboust et al., 2011, 2012). The metabasalt exposures of the Monviso unit vary greatly with some containing well-preserved carbonate-bearing pillow basalts and pillow breccias, and contain limited exposures of pelitic metasediments in contact with the metabasalts (also see Angiboust et al., 2012). The higher-grade Lago Superiore Unit contains rare exposures of relatively undeformed carbonate-bearing pillow basalts and pillow breccias with local intercalations of pelitic metasedimentary rocks.

Cervinia, Italy. The Zermatt-Saas ophiolite contains abundant pristine carbonate-bearing pillow basalts, pillow breccia, hydrothermalized basalts, and talc-schist serpentinites demonstrating little evidence of exhumation related retrogression (Angiboust et al., 2009; Angiboust and Agard, 2010). In addition, exposures near Cervinia contain trench-fill pillow basalts, ranging from mm- to m-scale, that are cemented in a carbonate-dominated matrix. While the metamorphic grade of this region (520-560°C and 2.2-2.4 GPa; Angiboust et al., 2009) overlaps with that of Monviso, Servette, and Clavalité Valley, the dominance of carbonate in contact with well-preserved basalts, limited degree of retrogression, and the abundant garnet-bearing rocks in the region are of interest in this study. Retention of oxidized and reduced C in the overlying metasedimentary rocks was investigated by Cook-Kollars et al. (2014).

Servette, St. Marcel and Clavalité Valleys, Italy (Zermatt-Saas). At this locality, exposures of pristine carbonate-bearing pillow basalts, pillow breccia, and hydrothermally altered basalts display chemical signatures of extensive seafloor alteration and contain abundant hydrothermal deposits (Martin and Tartarotti, 1989; Martin et al., 2008). These UHP eclogites contain pillow breccia with carbonate mineralogy varying from calcite to magnesite and often associated with chalcopyrite deposits. Peak *P-T* estimates (530-550°C and ~2.4 GPa), field maps, descriptions of the metabasalts, and a small number of whole-rock chemical data are presented by Angiboust and Agard (2010).

Lago di Cignana, Italy. The UHP metabasalts of Lago di Cignana are the highest-grade rocks investigated in this study (van der Klauw et al., 1997; see the petrologic studies of the metasedimentary rocks at this locality by Reinecke, 1991, 1998). Recent studies have shown evidence of micro-diamond inclusions within garnets from these metabasalts and represent peak *P-T* paths of ~600°C and ≥3.2 GPa (Groppo et al., 2009; Frezzotti et al., 2011). Exposures of siliceous and carbonate/pelitic sediments associated with the pillow basalts have previously been studied for evidence of decarbonation (Cook-Kollars et al., 2014). Carbonate-bearing inter-pillow regions and veins are not abundant at this locality (see van der Klauw et al., 1997); however, small amounts of finely disseminated carbonate in whole-rocks afford an opportunity to investigate carbonate retention to depths approaching those beneath arcs.

Tianshan , China. Mafic HP rocks of the Tianshan Mountains in western China allow study of devolatilization along the blueschist- and eclogite-facies transition in seafloor-altered basalts metamorphosed at 480-580°C, 1.8-2.1 GPa and in some areas UHP conditions of 500-630°C and 2.4-3.3 GPa (see **Fig. 1B**; Klemd et al., 2002; Wei et al., 2003). The HP/UHP unit is interpreted to reflect a tectonic mélange or accretionary wedge-like sequence, dominated by forearc

sediments. Peak metamorphism occurred at ~315 Ma with the main exhumation processes at ~311 Ma (Klemd et al., 2005, 2011). Detailed field and chemical studies (e.g., Gao and Klemd, 2003; John et al., 2008, 2012) have yielded insights into the prograde dehydration of blueschist to carbonate-bearing eclogite veins and multiple textural carbonate setting within the basalts that have seen relatively little exhumation overprinting (Gao and Klemd, 2003; Klemd et al., 2005; Beinlich et al., 2010). van der Straaten et al. (2012) presented a small C and O isotope dataset for HP metabasalts from Tianshan which rehydrated to blueschists during their exhumation along the plate interface and suggested that the low $\delta^{13}C$ values of some of the carbonates reflect the influence of fluid from a source containing organic/reduced C.

3. Methods

3.1 Carbon and Oxygen Isotope Analyses

Carbonate from various textural settings (see **Table 2**) was sampled by micro-drilling using 1 and 2 mm tungsten carbide bits (data in **Supplementary Tables 2,3**). The samples were analyzed on a Finnigan MAT 252 using a GasBench II and methods described by Cook-Kollars et al. (2014). Calcite, and where present, dolomite, ankerite, and magnesite, were reacted at 72°C for 0.5, 3, 3, and 6 hours (respectively) with 0.2 mL phosphoric acid to release CO_2. Unknowns were evenly spaced with analyses of a synthetic in-house carbonate standard and international standards NBS-18 and NBS-19. All samples were measured with six replicates following five reference gas peaks. Regular analysis of a house standard and international standard NBS-19 allowed monitoring and correction of the data, resulting in standard deviation (1σ) of ~0.2‰ for both $\delta^{13}C$ and $\delta^{18}O$. The $\delta^{13}C$ and $\delta^{18}O$ values are reported relative to VPDB and VSMOW, respectively.

A small number of analyses of reduced C were obtained by first removing carbonate using 1N HCl. Samples were then oxidized in sealed 6 mm (o.d.) quartz tubes and combusted with Cu-CuO_x reagent before extraction and analysis by dual-inlet methods (methods in Li and Bebout, 2005). Accuracy was ensured by analyzing the graphite standard USGS-24, for which repeated analyses yielded mean $\delta^{13}C$ of -16‰ with 1σ of <0.1‰. $\delta^{13}C$ is reported relative to VPDB.

3.2 Thermodynamic Modeling using Perple_X

Thermodynamic modeling was computed following the free-energy minimization approach using the software Perple_X (version 6.6.8, April 2013 version; Connolly, 2005) and the thermodynamic database of Holland and Powell (1998; with 2002 revision). Solution models (referred to as Do, Pheng, GlTrTsMr & GlTrTsPg, Gt, and Chl within the software) were used for carbonates, micas, amphiboles, garnet, and chlorite, respectively (Holland and Powell, 1998). Clinopyroxene stability was computed using the solution model by Gasparik (1989). Mineral end-member calculations for biotite, feldspar, and orthopyroxene were also considered but were not these phases were not stabilized at the selected *P-T* range and for the rock compositions investigated (compositions in **Supplementary Table 4**). The volatiles H_2O and CO_2 were considered as thermodynamic components (not a saturated phases) for the closed-system pseudosections and as saturated phases for the T-X_{CO_2} calculations. H_2O- and CO_2-bearing fluid behavior was modeled using the CORK equation of state by Holland and Powell (1991, 1998).

4. Results

4.1 Field Relations and Petrography

4.1.1 Metabasaltic Rocks

Generalized field textures and occurrences of carbonate at the sampling localities are presented in **Table 2**, with representative examples shown in the field photographs in **Fig. 2**. Most of the sampled exposures contain metabasaltic rocks showing little evidence for deformation at the macroscopic scale and containing clear pillow/interpillow structures and veins of varying textures, along with breccia, making it possible to sample carbonate from a variety of textural settings. Carbonate, mostly calcite, also occurs as a finely disseminated whole-rock phase and in relatively non-abundant micro- and macro-scopic scale veins and segregations. At the sites containing basaltic or gabbroic breccias, carbonate occurs as the dominant breccia filling (see **Fig. 2D**). Contacts of carbonate breccia fillings with metabasaltic clasts show no mineralogical evidence of metasomatic exchange — such metasomatism, had it occurred, might have driven some decarbonation (Thompson, 1975; Joesten, 1977; Ague and Rye, 1999; Bebout, 2013). Conspicuously absent in the W. Alps exposures are cm- to m-scale, through-going (i.e., at scales beyond those of individual small outcrops) veins indicating larger-scale fluid mobility (of the type described for Tianshan localities; Beinlich et al., 2010; John et al., 2012).

It is difficult to petrographically deduce mineralogical records of whole-rock decarbonation in the metabasalts, as the mineral assemblages are very similar to those expected as the result of HP/UHP metamorphism without any involvement of carbonate in prograde reactions. Calcium-rich phases that could in part reflect decarbonation of calcite or dolomite include garnet, omphacitic pyroxene, lawsonite, clinozoisite, as described in the previous petrologic studies of these localities cited in **Section 2**. **Sections 4.4 and 5.1.1** contain discussion of this complication and **Section 5.1.2** discusses the evidence for little or no decarbonation, and closed-system behavior, provided by the C and O isotope compositions of the rocks.

The carbonate sampled for this study, and analyzed for its C and O isotope compositions, is from a variety of textural settings (see **Table 2**, **Supplementary Table 2**). Many of the metabasaltic rocks contain 1-5 wt. % finely disseminated carbonate, in some cases not visible petrographically, but the dominant reservoirs for carbonate are in small-scale (<50 μm wide) veins of varying textures, breccia matrices, and interpillow regions. In some samples, μm to mm scale pods and veinlets are discontinuous beyond the scale of individual thin sections (several tens of mms), whereas others are through-going beyond this scale (up to cm and m scales) in rocks lacking penetrative deformation fabric. Some breccias contain >25% carbonate by volume (see example in **Fig. 2D**), again, showing no obvious mineralogical evidence of reaction between the carbonate and the silicate mineral assemblages in the metabasaltic or metagabbroic clasts.

4.1.2 Ultramafic Rocks (Ophicarbonates)

The ophicarbonate exposures sampled in this study, across all grades, are mostly breccias with variably metasomatized serpentinite clasts (cm to m scales) and extremely abundant carbonate as breccia filling and veins (together, up to 30 vol. % of some exposures) showing a wide range of textures indicating their stages of evolution. At a few of the localities, the ophicarbonates show the development of later-stage, more penetrative cleavage, in some cases with intensely foliated rocks in which breccia textures are largely destroyed and nearby domains of non-foliated breccia, separated by deformation "fronts." The contacts between these highly deformed and undeformed ophicarbonates can be quite sharp, with strong gradients in extent of foliation over cm scales. The more foliated rocks tend to contain few veins cross-cutting their foliation.

4.2 Carbon and Oxygen Isotope Compositions of Carbonate (and Reduced Carbon) in Metabasaltic Rocks

346 Carbon and O isotope compositions for the metabasaltic rocks are shown in the compilation
347 in **Fig. 3** (see **Supplementary Table 2** for textural occurrences of individual samples) and for
348 individual sampling localities in **Fig. 4**. The carbonate occurrences at individual localities tend to
349 show variation related to the textural setting of the carbonate, but there is significant overlap
350 among the datasets for the various localities. Also shown in **Fig. 3** are ranges in C and O isotope
351 compositions of finely disseminated (whole-rock) calcite in various altered basalts on the modern
352 Atlantic seafloor (from Furnes et al., 2001) and data for calcite veins in seafloor-altered basalts
353 (from Alt and Teagle, 2003; Coggan et al., 2010; R. Coggan, pers. comm., 2014). The data for
354 the veins and finely disseminated calcite tend to have $\delta^{13}C$ similar to, but $\delta^{18}O$ lower than, values
355 for carbonate from similar textural settings in basalts on the modern seafloor. However, the $\delta^{18}O$
356 values mostly fall within the range of whole-rock values for altered oceanic crust (+5 to +20‰,
357 mostly +5 to +10‰; from Alt and Teagle, 2003; Alt, 2004). The data for the Zermatt-Saas area
358 (~+9 to +20‰; green-filled symbols in **Fig. 3**) show the widest range in $\delta^{18}O$, encompassing the
359 smaller ranges for the other units among which there is more limited overlap.
360 Several suites demonstrate differences in whole-rock values and values for carbonate
361 sampled from various other textural settings by micro-drilling. Carbonate in the lowest-grade
362 (prehnite-pumpellyite facies) metabasalts, from the Bracco unit, have $\delta^{13}C$ of -4.5 to +2.0‰ and
363 $\delta^{18}O$ values of +16 to +21.3‰. Excluding several whole-rock samples (red-filled squares), the
364 data for the Bracco Unit range in $\delta^{13}C$ values from -1.5 to +2.0‰ and show fairly uniform $\delta^{18}O$
365 of +16 to +17.3‰ (see **Fig. 4A**). Increasing in grade, discontinuous veins and pods in Mt.
366 Figogna Unit metabasalts have $\delta^{13}C$ values of -0.2 to +0.8‰ and $\delta^{18}O$ values of +12.4 to
367 +13.2‰, with one whole-rock sample having higher $\delta^{18}O$ near +17‰ (**Fig. 4A**). Approaching
368 the blueschist facies, whole-rock analyses from the Cravasco-Voltaggio unit display $\delta^{13}C$ values

of -2.6 to +0.8‰ and $\delta^{18}O$ values of +18.0 to +25.8‰ (see **Fig. 3**). Blueschist-facies metabasalts from Ubaye Valley, France, display large variation in whole-rock $\delta^{13}C$ of -12 to +0.3‰, for whole-rock carbonate showing a correlation with $\delta^{18}O$ ranging from +15.1 to +24.9‰ (see this trend in **Fig. 4C**). However, discontinuous and through-going veins have $\delta^{13}C$ of -5.1 to +2‰ and a tighter clustering in $\delta^{18}O$ of +14.0 to +16.9‰. Carbonate from various textural settings in rocks from the Lago Superiore unit at Monviso contain $\delta^{13}C$ values of -0.8 to +2.5‰ and $\delta^{18}O$ values of +8.5 to +15.9‰ (**Fig. 4B**). Through-going veins (green-filled diamonds) are relatively uniform in $\delta^{18}O$ (+11.5 to +12.5‰) and define a curved array between endmember $\delta^{13}C$ values of +2.5‰ and -0.8‰. The Monviso unit at Monviso contains carbonate with $\delta^{13}C$ of -0.4 to +1.2‰ however, with $\delta^{18}O$ values of +12.4 to +15.0‰ higher than those of most Lago Superiore carbonate. Metabasalts from the Zermatt-Saas ophiolite show clustering of $\delta^{13}C$ values between -1.6 and +1.9‰ while having a broad range of $\delta^{18}O$ values of +9.1 to +19.2‰, showing little relationship with varying textures (**Fig. 4D**). The highest-grade metabasalts, at Lago di Cignana (UHP), display a wide range of whole-rock $\delta^{13}C$ values spanning from -6.1 to +0.7‰ and $\delta^{18}O$ values of +11.5 to +21.9‰, producing a linear array (red-filled squares in **Fig. 4D**).

Eclogites from the Tianshan show a wide range of carbonate $\delta^{13}C$, from -14.1 to +2.8‰, whereas $\delta^{18}O$ shows a smaller range of +9.9 to +15.8‰, and these data (for whole-rocks and discontinuous pods) form a strong trend (see the black arrow on the left in **Fig. 3**). These samples represent three traverses, one the envelope of a large vein (fluid conduit; see Zack and John, 2007) and the others of rocks partially rehydrated during fluid-rock interaction along the plate interface (see van der Straaten et al., 2008, 2012). The data for metabasalts in the Catalina Schist (from Bebout, 1995) similarly show a range of $\delta^{13}C$ to values considerably lower than those expected for seafloor alteration, at relatively uniform $\delta^{18}O$. Among the sample suites for the

localities in Italy and France, only Ubaye and Lago di Cignana show well-defined trends, in both cases toward higher $\delta^{18}O$ and lower $\delta^{13}C$ values approaching -15‰ (**Figs. 3, 4C,D**).

Several of the higher-grade metabasaltic samples were analyzed for their C concentrations after pre-treatment with HCl (to dissolve carbonate), using sealed-tube methods commonly employed for analyses of organic/reduced C (see **Section 3.1**). Analyses of two Zermatt-Saas metabasalts yielded concentrations of 0.12 and 0.04 wt. % C with $\delta^{13}C$ of -22.4 and -26.7‰, respectively, and one Monviso UHP metabasalt yielded a C concentration of 0.07 wt. % (700 ppm) with $\delta^{13}C$ of -5.1‰.

4.3 Carbon and Oxygen Isotope Compositions of Carbonate in Ophicarbonates

Carbon and O isotopes for carbonate in ophicarbonates are shown in **Fig. 5** (see data in **Supplementary Table 3**) compared to compositions of ophicarbonates from various settings, including the seafloor, presented in Clerc et al. (2014). Most of the samples have $\delta^{13}C$ in the range of +0.3 to +3.0‰, but show varying ranges and relationships in their $\delta^{18}O$. The highest-grade units (Voltri Massif, Zermatt-Saas) show the most tightly scattered and lowest values of $\delta^{18}O$ (+9.9 to +12.6‰).

The prehnite-pumpellyite facies Bracco unit ophicarbonates contain a range in $\delta^{13}C$ values of +0.6 to +2.8‰ and $\delta^{18}O$ values of +14.4 to +22.2‰, showing no obvious trends. Slightly increasing in grade, several samples of ophicarbonates from the Mt. Figogna unit tightly cluster in $\delta^{13}C$ values of +0.7 to +1.2‰ and $\delta^{18}O$ values of +14.0 to +14.9‰. Comparable in grade with Mt. Figogna, ophicarbonates from nearby Montaretto have $\delta^{13}C$ values of +1.0 to +2.6‰, however, show a broad range of $\delta^{18}O$ values from +15.1 to +24.6‰ (also see Schwarzenbach et al., 2013). Blueschist-facies ophicarbonates from Ubaye Valley, France, display the largest range in $\delta^{13}C$ values of the suites we investigated, spanning from -3.0 to +1.8‰ and $\delta^{18}O$ values of

+16.0 to +25.4‰. Interestingly, the metabasaltic carbonate for Ubaye also shows this range to low $\delta^{13}C$ (see **Figs. 3, 4C**). Eclogite-facies ophicarbonates from the Zermatt-Saas ophiolite span a range in $\delta^{13}C$ values from -0.4 to +3.0‰ with a narrow range of $\delta^{18}O$ values (+9.9 to +12.6‰). Data for ophicarbonates from the Voltri Massif fall within the range of data for the Zermatt-Saas ophiolite, the other higher-grade (eclogite-facies) locality, with $\delta^{13}C$ values of +0.9 to +1.8‰ and $\delta^{18}O$ values of +10.1 to +11.3‰.

In general, the arrays of O and C isotope data for ophicarbonates and metabasalts from the same locality tend to overlap but show considerable differences in distribution (compare **Figs. 3 and 4**). For example, for the Bracco Unit, data for metabasalts show relatively uniform $\delta^{18}O$ +16 to +17.5‰) and $\delta^{13}C$ ranging from -1.5 to 2.0‰. The ophicarbonates from the same locality have $\delta^{13}C$ of +0.5 to +3.0‰ and a show a wider range in $\delta^{18}O$ of ~+13.8 to +21.5‰. As another comparison, the Zermatt-Sass metabasalt carbonate ranges widely in $\delta^{18}O$, from +9 to +20‰, with $\delta^{13}C$ of -2.5 to +2‰. The ophicarbonate from the Zermatt-Saas shows a far more narrow range in $\delta^{18}O$ but $\delta^{13}C$ of -0.5 to +3.0‰ that largely overlaps the $\delta^{13}C$ range for the metabasalts.

4.4 Thermodynamic Modeling of the Devolatilization of the Metabasalts and Ophicarbonates

Pseudosections for four MORB compositions representing closed systems, generated using Perple_X, are shown in **Fig. 6** (the system modeled was NCKFMASH+CO_2; compositions are provided in **Supplementary Table 4**). The bulk compositions modeled in these calculations were selected to represent a wide range of alteration states and carbonate concentrations of seafloor-altered basaltic rocks (see Alt, 2004), with the composition for basalts at ODP Site 417/418 representing the most altered rocks. On these figures, dashed white lines represent an array of cool to warm modern-day subduction zone *P-T* paths from Syracuse et al. (2010) and van Keken et al. (2011; also P. van Keken, personal communication, 2013). The most significant

changes in mineralogy, representing significant devolatilization, are shown with large dashed lines and arrows. For greater simplicity, minor oxide occurrences, as well as carbonate mineralogy, are excluded from the field labels. On these figures, the spectrum of colors represents CO_2 concentration and, on each, these concentrations show little change along lower-P, forearc parts of the *P-T* paths and significant decrease beginning at about 600˚C and at pressures of 2.0 to 2.75 GPa corresponding to 60-90 km depths.

Figure 7 shows the calculated modal abundances of major silicate minerals and carbonates from the average composition of ODP core 417/418 (Staudigel et al., 1996) along the subduction zone *P-T* paths for the four modern margins shown in **Fig. 6C** (paths from Syracuse et al., 2010; van Keken et al., 2011; P. van Keken, personal communication, 2013). To simplify the figure, minor mineral occurrences are omitted and carbonate mineralogy is indicated as an aggregate. Along each *P-T* path, garnet crystallization increases mostly at the expense of lawsonite. A decrease or loss of carbonates is coupled with the increase in clinopyroxene and to a lesser degree garnet. Glaucophane breakdown produces no changes in the modal abundances of major minerals or carbonates. Based on these variations in modal abundances, generalized reactions along these paths are likely to be of the following generalized types:

Reaction occurring prior to breakdown of carbonate:

glaucophane + garnet = clinopyroxene + H_2O (**Figs. 7A,B,C)** **(1)**

Reactions involving breakdown of carbonate:

lawsonite + clinopyroxene + carbonate = garnet + H_2O + CO_2 (**Figs. 7A,B**) **(2)**

garnet + carbonate = clinopyroxene + CO_2 (see **Figs. 7C,D**) **(3)**

Note that, for all *P-T* paths, lawsonite is produced prior to significant carbonate breakdown, thus presumably not via a decarbonation reaction. Glaucophane is not stabilized along the

warmest *P-T* path, that for Cascadia (see **Fig. 7C**). Along all paths, beyond ~2.5 GPa, a bulk composition such as this (ODP Site 417/418) would stabilize a classic eclogite assemblage of clinoproxene+garnet largely devoid of volatiles, other than CO_2 in any residual carbonate, unless phases such as phengite are stabilized by small amounts of K_2O incorporated during seafloor alteration (see Bebout, 2007a). The superposition of these calculations and the various *P-T* paths show that, in the unlikely case where the released volatiles are still present (i.e., have not physically left the rock/system), some re-incorporation is possible at >3.0 GPa.

Figure 8A shows isopleths of H_2O and CO_2 for the closed-system model of the more altered rock composition from ODP core 417/418 (see **Figs. 6C,7**), the peak *P-T* estimates for the metabasaltic sites sampled in this study (shaded rectangular regions; see **Fig. 1B**), and the modern-day subduction *P-T* paths from **Fig. 6**. Significant dehydration (~65%) is evident for the higher-grade suites studied here but little or no decarbonation is indicated for prograde metamorphism to these peak conditions. Along the *P-T* paths for the various modern margins, excluding the path for the very warm Cascadia margin, decarbonation reaction begins to occur at temperatures of ~600˚C and the maximum extents of decarbonation experienced by rocks along these paths are 7% for Tonga, 43% for Northern Vanuatu, and 100% for Nankai (the latter also a relatively warm margin). **Figure 8B** shows profiles of H_2O and CO_2 wt. %, plotted vs. pressure, for a cool margin (Tonga), a margin intermediate in its *P-T* path (Northern Vanuatu), and a warm margin (Cascadia). On this figure, it is again clear that varying degrees of dehydration occur along earlier parts of these paths and to the peak-metamorphic *P-T* conditions for the units we sampled. As shown in **Fig. 7**, this H_2O loss is largely due to the breakdown of glaucophane and/or lawsonite giving way to clinopyroxene. The more significant losses of CO_2 along the

paths for Marianas, Northern Vanuatu, and Cascadia (see **Figs. 7B,C,D**) correspond to increase in the abundance of clinopyroxene.

The effect of infiltration by extremely H_2O rich fluids on mineral reaction for the composition representative of ODP Site 417/418 (from Staudigel et al., 1996) is demonstrated for two pressures (1.5 and 2.5 GPa) in the T-X_{CO_2} diagrams in **Fig. 9**. On these figures, carbonate is again simplified for clarity. **Figures 9A and B** present the same ranges in X_{CO_2} values at pressures of 1.5 and 2.5 GPa (respectively) and panels 1-4 below show the modal abundances calculated for along pathways toward lower X_{CO_2} at two temperatures (450 and 550˚C) at each pressure (see the arrows pointing from higher to lower X_{CO_2}). As for the closed-system calculations, garnet crystallization largely occurs at the expense of lawsonite. The dramatic losses of carbonate are accompanied by large increase in clinopyroxene abundance and, at the higher temperature, also some increase in the abundance of garnet. In the calculation for 1.5 GPa and 550˚C, the decrease in the abundance of carbonate is more gradual than in the three other calculations and is accompanied by decrease in lawsonite abundance and increased abundance of garnet and, to a lesser extent, glaucophane.

Figure 10 shows a calculation of H_2O and CO_2 wt. % as a function of extents of devolatilization for an ophicarbonate composition and the *P-T* paths also used in **Figs. 6 and 8**. The peak *P-T* estimates for the ophicarbonates investigated in this study are shown as dark-shaded boxes and it is evident from this calculation that, in a closed system, little or no decarbonation would be expected. In the modern margins represented by the four *P-T* paths on **Fig. 10**, modest amounts of decarbonation would be expected over the 2.0 to 3.0 GPa interval.

5. Discussion of Results

Our integrated field, petrologic, theoretical, and geochemical approach allows a broad consideration of the extent to which C is retained in metabasaltic and metaultramafic rocks subducted to depths approaching those beneath arc volcanic fronts. Here, it is again worth noting that our work was conducted on large, relatively coherent/intact exposures of metabasaltic rocks and ophicarbonates, for the most part without obvious shear zones, and that with the exception of the Tianshan exposures we investigated, these exposures tended not to contain larger, more through-going vein sets indicative of open-system behavior. In **Section 5.3**, we discuss the need for further investigation of the significance of infiltration-driven C release in shear zones, at or near the subduction interface, in the overall flux of C from subducting slab+sediment sections.

5.1 Metabasaltic Rocks

5.1.1 Field Relations and Petrography of the Metabasaltic Rocks

Preservation of abundant carbonates in the relatively undeformed metabasalts, particularly in pillow/interpillow structures and pillow breccias, demonstrates the widespread retention of CO_2 (**Table 2**) in Italian/French Alps HP/UHP metabasalts subducted to depths of up to 90 km (**Fig. 2**). This evidence for the retention of carbonate is consistent with observations made in previous studies (e.g., Barnicoat and Cartwright, 1995; Rubatto et al., 1998; Cartwright and Barnicoat, 1999, 2003; Miller and Cartwright, 2000) and argues against the extensive decarbonation calculated for open-system models by Gorman et al. (2006). For the Italian localities/units investigated in our study, the absence of more through-going, macroscopic-scale veins, and the lack, for most exposures, of convincing mineralogical or isotopic evidence for pervasive infiltration by externally-derived fluids, would seem to preclude significant CO_2 mobilization by carbonate dissolution documented for several exposures on Syros and Tinos (Greek Islands) by

Ague and Nicolescu (2014). Unlike the larger, through-going veins in the Tianshan (investigated by Beinlich et al., 2010; John et al., 2012; van der Straaten et al., 2012), which do show evidence for carbonate mobility, the veins in the Italian exposures do not show obvious leaching or addition of carbonate in well-developed envelopes. However, it is possible that small amounts of carbonate were dissolved by infiltrating fluids, particularly from rocks showing evidence of control of their isotopic compositions from an external reservoir (e.g., metabasalts showing tight ranges in $\delta^{18}O$ or correlated shift in $\delta^{18}O$ and $\delta^{13}C$; see **Figs. 3,4**; see discussion of this possible open-system behavior in **Section 5.1.2**). Small amounts of carbonate dissolution, distributed over very large rock volumes, could constitute significant mobilization of C from or within slabs.

Petrographic/mineralogical identification of decarbonation in the HP/UHP metabasalts is made difficult by the fact that the mineral phases produced by such reactions are stabilized without the need for involvement of carbonates (see the calculations in **Fig. 6** for basalts containing a wide range of initial CO_2 concentrations). However, for a small number of samples, from Ubaye and Tianshan, possible evidence of decarbonation occurs as reaction rims at contacts between mafic breccia clasts and carbonate cement. Within pillow matrices, across the wide-range of *P-T* represented by our localities, carbonate is predominantly finely disseminated and displays little evidence of reaction with surrounding silicates to produce calc-silicate phases and release CO_2. In a small number of metabasalts, discontinuous carbonate-bearing veins show reaction rims with amphibole, epidote, and omphacite, pointing to local-scale metasomatic reaction possibly involving CO_2. The surprisingly small number of through-going carbonate-bearing veins in these relatively undeformed metabasaltic exposures (most of them preserving pillow textures; see **Table 2**; **Figs. 2A-C**) is suggestive of limited degrees of large-scale fluid-flow (i.e., fluid mobility at scales greater than the individual outcrops).

5.1.2 Isotopic Evidence for Closed to Limited Open-System Behavior during Subduction-Zone Metamorphism of the Metabasaltic Rocks

The C and O isotope data for the metabasalts (see **Figs. 3,4**) allow some assessments of extents of open- and closed-system behavior and, where open-system behavior is indicated, the compositions and possible sources of the externally-derived fluids. In this discussion of the isotopic data, we do not consider in detail the consequences of having minor amounts of dolomite, ankerite, or siderite in some samples, in addition to the far more abundant calcite. Fractionation of C (and O) isotopes among these phases is minor, near 0.5‰ ($10^3 \ln\alpha$), over the temperature range of 400-600˚C (see Sheppard and Schwarz, 1970).

The majority of the suites retain carbonate $\delta^{13}C$ overlapping with that of carbonates produced during seafloor alteration; however, the $\delta^{18}O$ values are significantly lower than those for the seafloor carbonates (see **Figs. 3, 4**). Although shifts to lower $\delta^{18}O$ could be accomplished through open-system behavior, involving infiltration by fluids from external sources, we suggest that (particularly for the finely disseminated carbonate, micro-veins, and segregations) these shifts could be the result of more closed-system exchange between the carbonate and the modally dominant silicate mineral assemblage. Calculation of equilibration of calcite $\delta^{18}O$ with clinopyroxene and garnet, at 500-600˚C, in a fictive eclogite with whole-rock $\delta^{18}O$ of +10‰ (using fractionation factors from Zheng, 1993) yields values near +13‰ within the range of observed values for the finely disseminated carbonate (see **Fig. 3**). A number of other authors have concluded that HP/UHP metabasaltic rocks can behave largely as closed systems during metamorphism, based in part on O isotope compositions (see Barnicoat and Cartwright, 1995; Cartwright and Barnicoat, 1999, 2003; Miller et al., 2001; Nadeau et al., 1993; Philippot, 1993).

574 Decarbonation involving finely disseminated calcite in the metabasalts would be expected to
575 produce lowering of $\delta^{13}C$, with or without change in $\delta^{18}O$, the O shifts depending on the extents
576 to which the decarbonation is driven by infiltration by externally-derived H_2O-rich fluids. For the
577 closed-system case, with no infiltration, decreases in $\delta^{18}O$ due to decarbonation are strongly
578 limited by the relatively small fractions of O removed in the CO_2 (i.e., the large fraction of O left
579 in the residue in silicate phases and any residual carbonate). For extensive decarbonation of
580 finely disseminated carbonate, where the fraction of C remaining approaches 0, shifts of up to
581 10‰ or greater are possible by a Rayleigh distillation process (see Valley, 1986). One
582 representative path in O-C isotope composition that residual carbonate might take for a Rayleigh
583 process is shown in **Fig. 3**. It would be difficult to identify the small shifts in $\delta^{18}O$ potentially
584 associated with closed-system decarbonation, given the very large range of possible starting $\delta^{18}O$
585 values related to seafloor alteration (see Alt et al., 1996; Alt and Teagle, 2003; Furnes et al.,
586 2001) and the superimposed exchange with silicate phases. However, the lack of shift of $\delta^{13}C$ to
587 beyond the range expected for seafloor-altered basalts, observed for most of the metabasaltic
588 suites, is consistent with little or no decarbonation. For the case of an infiltrating extremely C-
589 poor, H_2O-rich fluid driving decarbonation reaction, any $\delta^{13}C$ shift would be purely the result of
590 decarbonation, and the exact direction and magnitude of $\delta^{18}O$ shift would depend on the $\delta^{18}O$ of
591 the fluid and the temperature at which the residual carbonate equilibrated with that fluid.
592 For a few of the suites, isotopic compositions are indicative of some open-system behavior
593 and, in some cases, consistent with equilibration with fluids derived in nearby metasedimentary
594 rocks (see the data for these metasedimentary sections in Cook-Kollars et al., 2014). The
595 relatively uniform $\delta^{18}O$ for veins in the low-grade Bracco Unit (**Fig. 4A**) indicates the possibility
596 of some control of isotopic compositions by exchange with an externally-derived fluid with

relatively uniform $\delta^{18}O$ but that did not result in $\delta^{13}C$ differing from that typical for seafloor altered basalts. Some whole-rock carbonate in these metabasalts (red-filled squares) is considerably higher in $\delta^{18}O$ and shows a wide range of $\delta^{13}C$ values, perhaps reflecting differential control by infiltrating fluids and greater preservation of isotopic compositions inherited from the seafloor or influenced by some decarbonation (the latter producing shift to lower values). Whole-rock, finely disseminated carbonate in blueschist metabasalts from the Ubaye Valley shows shifts towards more organic-rich $\delta^{13}C$ signatures (**Fig. 4C**), perhaps in part reflecting decarbonation (see discussion above), and correlated shift to higher $\delta^{18}O$. These shifts could reflect exchange with externally-derived, C-bearing, H_2O-rich fluids, with or without some shift associated with decarbonation. Similar relationships are exhibited by whole-rock data for very low-carbonate UHP metabasalts from Lago di Cignana. Data for more through-going veins in the Lago Superiore Unit at Monviso (green-filled diamonds in **Fig. 4B**) show a modest range of $\delta^{13}C$ but a very narrow range of $\delta^{18}O$, the latter perhaps reflecting control of O isotope composition by fluids with uniform $\delta^{18}O$ from an external source. The range in $\delta^{13}C$ of these Lago Superiore veins contrasts with the far larger ranges in $\delta^{13}C$, at fairly uniform $\delta^{18}O$, seen for the Tianshan and Catalina Schist metabasalts (see **Fig. 3**). The data for these latter two suites could reflect exchange with fluids with uniform $\delta^{18}O$ but that previously equilibrated differentially with organic-rich sediments during entrainment into a shear zone (for some samples, perhaps with some superimposed isotopic effects of decarbonation; for Catalina Schist, see Bebout, 1995).

For some of the Alps suites, the $\delta^{18}O$ of calcite showing relatively narrow ranges, without appreciable shift in $\delta^{13}C$ from the range for altered seafloor basalts, differs significantly from the calcite $\delta^{18}O$ values in nearby calc-schists of similar grade that could perhaps be viewed as

potential fluid sources. The best examples of this relationship are the subset of MV-LS samples showing more through-going textures (green-filled diamonds in **Fig. 4B**; $\delta^{18}O$ near +12‰) and data for various vein types at the Bracco Unit localities ($\delta^{18}O$ near +16.5‰). Neither of these isotopic compositions is consistent with equilibration with carbonate from the calc-schists (via fluids), which at these grades has $\delta^{18}O$ near +18‰ (Monviso) and +25‰ (estimated for Bracco; see Cook-Kollars et al., 2014). The lower-$\delta^{18}O$ fluids producing these arrays could have been mixtures of fluids from the calc-schists and metapelites and from another source such as dehydrating mafic or ultramafic rocks at greater depths in the subduction zone. In contrast, the trends toward higher $\delta^{18}O$ and lower $\delta^{13}C$ for some of the samples from the Ubaye Unit and the Zermatt-Saas localities (the gray-shaded diagonal arrow in **Fig. 3**) are more consistent with a shift toward equilibrium with fluids equilibrated with the metasedimentary section.

5.1.3 Theoretical Evidence for Decarbonation History of the Deeply Subducted Metabasalts

The thermodynamic calculations for closed systems presented in this paper, and by Kerrick and Connolly (2001b), indicate that very little decarbonation would occur at forearc depths along the *P-T* metamorphic gradient investigated in this study, and along forearc *P-T* paths experienced in most modern subduction margins. For the compositions considered in this study, and by Gorman et al. (2006), significant decarbonation occurs only at very low X_{CO_2}, a condition that seemingly would require infiltration of the rocks by H_2O-rich fluids. For depths greater than those investigated in these field localities (i.e., >90 km), even the closed-system calculations indicate significant decarbonation, depending on the *P-T* path the rocks experience (**Figs. 6, 8**). Use of the more recently published *P-T* paths (Syracuse et al., 2010; van Keken et al., 2011) produces far larger CO_2 loss over the depth interval of 80-120 km than was suggested by Kerrick

642 (2001a,b), who considered earlier models that did not take into account the heating of slabs by
643 the convecting mantle wedge.
644 These calculations for the metabasaltic rocks would permit infiltration of the metabaslts by
645 fluids that were H_2O-rich (i.e., had high O/C) but had X_{CO_2} higher than that required to drive
646 decarbonation reaction. This scenario would conceivably produce shifts in carbonate $\delta^{18}O$
647 without as obvious a shift in $\delta^{13}C$ (see the arrow in **Fig. 3** labeled "Exchange with H_2O-Rich
648 Fluid"), depending on the $\delta^{18}O$ of the fluid, the temperature of equilibration, and to a lesser
649 extent, the carbonate mineralogy. Some of the metabasaltic suites, particularly Ubaye and
650 Cignana (see **Figs. 3,4**), could have been shifted to higher $\delta^{18}O$ and lower $\delta^{13}C$ by a C-bearing
651 infiltrating fluid with X_{CO_2} insufficiently low to drive decarbonation reaction (see **Fig. 9**). As
652 noted in **Section 5.1.2**, for many of the metabasalts, the shifts in $\delta^{18}O$ of whole-rock carbonate
653 (finely disseminated and in small pods and discontinuous veinlets) are consistent with isotopic
654 exchange of the carbonate with the more abundant silicate phases in these rocks, thus seemingly
655 requiring no influence by externally-derived fluids.
656 ***5.2 Metaultramafic Rocks***
657 The highly carbonated metaultramafic rocks (ophicarbonates) investigated here show little
658 or no mineralogical evidence of decarbonation, consistent with the theoretical calculations of
659 Kerrick and Connolly (1998), and in **Fig. 10**, for prograde reaction in closed systems. Field and
660 petrographic study demonstrates retention of carbonate, for example, with little to no evidence of
661 reaction of carbonate with ultramafic clasts at macro- and micro-scopic scales. In a number of
662 the ophicarbonate exposures, the lack of foliation, retention of breccia cement textures
663 resembling those produced by seafloor alteration, and lack of more through-going veins are
664 consistent with a lack of larger-scale carbonate mobility during subduction. The localization of

665 any subduction-zone deformation along discrete shear zones allows preservation of original
666 breccia textures in more intact and undeformed zones, and the isotopic compositions of these
667 features overlap with those of ophicarbonate produced on the seafloor (see **Fig. 5**; cf.
668 Schwarzenbach et al., 2013). The wide range of C and O isotope compositions for seafloor
669 ophicarbonate (the protoliths) complicates identification of change due to subduction zone
670 metamorphism. However, the $\delta^{13}C$ values do not show obvious evidence for decarbonation (see
671 the typical Rayleigh trend for decarbonation in **Fig. 3**), supporting the mineralogical evidence for
672 a lack of such reaction. As for some of the metabasalts (e.g., Monviso; see **Fig. 4B)**, the highest-
673 grade ophicarbonates (particularly Voltri-Massif and Zermatt-Saas) show relatively narrow
674 ranges in $\delta^{18}O$ that could reflect the influence of a fluid from an external source. Lowering of the
675 $\delta^{13}C$ of some samples in these suites, particularly Ubaye, hints at the influence of organic C in
676 the fluid source, perhaps via exchange with nearby metasedimentary rocks (as for metabasalts
677 from the same locality; see **Figs. 3,4C**). Ophicarbonates from the lower-grade suites (Bracco, Mt.
678 Fignona, and Ubaye) show wide ranges in $\delta^{18}O$ perhaps consistent with greater preservation of
679 seafloor alteration signatures. Combining the field, petrographic, isotopic and theoretical
680 evidence, it appears that the ophicarbonates behaved as relatively closed systems, at the high
681 grades perhaps with some episodic infiltration by fluids from external sources insufficient to
682 drive appreciable decarbonation. This implies that a large fraction of the carbonate incorporated
683 into such rocks at/near the seafloor can be retained to great depths in subduction zones, perhaps
684 to 90 km.

685 Comparison of our calculations for ophicarbonates with those of Kerrick and Connolly
686 (1998) demonstrates the strong dependence of calculated decarbonation on the rock composition
687 employed in the calculations. Both the calculations in **Fig. 10** and by Kerrick and Connolly

(1998) indicate that such rocks would largely retain carbonate when subducted along a forearc *P-T* gradient such as that represented by our HP/UHP rocks and experienced in many modern subduction zones (example *P-T* paths shown in **Fig. 10**). However, the increase in temperature at the top of the slab and sediments caused by exposure to the convecting mantle wedge (at 80-120 km depths; see **Fig. 10**) could result in appreciable decarbonation and the calculations by Kerrick and Connolly (1998) show far more dramatic loss of CO_2 during this heating than our calculations in **Fig. 10**. For the composition modeled in Fig. 1A of Kerrick and Connolly (1998), nearly 100% loss of CO_2 would be predicted along a *P-T* path similar to that for N. Vanuatu.

5.3 Implications for Deep Subduction-Zone Carbon Cycling

In this study, as in the studies by Bebout et al. (2013) and Cook-Kollars et al. (2014), focus is placed on understanding devolatilization history of relatively "intact" volumes of lithologies thought to be subducting into modern margins. These exposures contain few through-going, larger vein networks and, for the most part, metabasalts and ophicarbonates do not show the development of penetrative deformation textures (e.g., containing intact pillow structures). All suggestions are that intact slabs and sediment sections would tend to behave as relatively closed systems except along the more extensive fracture networks and in other particularly deformed zones (e.g., shear zones) that would channelize dehydration-related fluid release (e.g., Zack and John, 2007; John et al., 2012; Konrad-Schmolke and Halama, 2014; Fusseis et al., 2009).

A number of authors have proposed relatively closed-system behavior during prograde metamorphism of less-deformed tracts of HP/UHP metabasaltic rocks and many of these studies were focused on metabasalts in the European Alps. Philippot and Selverstone (1991), Barnicoat and Cartwright (1995), Cartwright and Barnicoat (1999), Spandler et al. (2011; these authors suggested some limited open-system behavior), Nadeau et al. (1993), Widmer and Thompson

712 (2001), and Rubatto and Hermann (2003) all invoked relatively local-scale control over fluid
713 composition and little infiltration of mafic meta-ophiolitic rocks by externally-derived fluids (see
714 the discussion by Scambelluri and Philippot, 2001). More recently, Angiboust et al. (2011; 2014)
715 have identified brecciated and sheared domains, within the Monviso Massif, that likely represent
716 fluid channelways within large intact volumes of subducting ophiolite. Longer-distance fluid
717 flow through localized fluid conduits in coherent slab sections and at the subduction interface has
718 been proposed for a number of other HP/UHP localities (e.g., Herms et al., 2012, Ecuador; John
719 and Schenk, 2003, Zambia; Gao et al., 2007, Beinlich et al., 2010, John et al., 2012, and Li et al.,
720 2014, Tianshan; Spandler and Hermann, 2006, New Caledonia; Breeding et al., 2004; Miller et
721 al., 2009, Cyclades; Ague and Nicolescu, 2014, Corsica). This proposed focusing of fluid flow
722 (and related metasomatic alteration) in highly sheared and fractured zones echoes conclusions
723 from study of the Catalina Schist (California), in which metasomatism and isotopic
724 homogenization was enhanced in such zones (Bebout, 1991a,b; Bebout and Barton, 1993; King
725 et al., 2006, 2007) and larger volumes of less permeable, less-deformed metasedimentary and
726 metamafic rock behaved as closed systems (Bebout and Fogel, 1992; Bebout and Nakamura,
727 2003). The extent to which enhanced C loss along these more strongly deformed zones
728 contributes to the overall C flux from subducting top-slab sections requires further field
729 investigation. The studies of C mobility along such structures have tended to be conducted on
730 individual or small numbers of exposures and an assessment of the broader significance of such
731 loss will need to be conducted on a more regional scale.

732 Very simply considered, a loss of 10% of initially subducted C to forearc devolatilization
733 reactions implies delivery of 90% of this C inventory to depths beneath arcs, where another
734 fraction could be extracted to contribute to arc CO_2 degassing and other forearc and mantle

735 wedge C reservoirs. Loss of another 40% of the C beneath arcs would imply that 50% of the C
736 could be contributing to mantle regassing on modern Earth. However, this simple comparison
737 overlooks the likely inefficient delivery of any CO_2 released from subducting slabs into arc
738 source regions and ultimate return of this CO_2 to the atmosphere. Considerable amounts of C
739 could be transported updip toward the seafloor, along the subduction thrust, or stored in the
740 forearc or subarc mantle wedge.

741 **Table 3** provides estimates of extents of closed-system CO_2 loss, due to decarbonation
742 reactions, as rocks traverse the 80-120 km depth range over which the increased heating occurs
743 by exposure to the convecting part of the mantle wedge. These losses are based on the
744 calculations in **Figs. 6-8 and 10** in which the calculated *P-T* paths for the top of the slab in
745 selected modern Earth subduction zones (Cascadia, Nankai, Northern Vanuatu, and Tonga) are
746 superimposed on calculated closed-system reaction history for metabasalt and ophicarbonate.
747 Cook-Kollars et al. (2014; see their Supplementary Fig. 3) similarly superimposed these thermal
748 models on the closed-system calculations of Kerrick and Connolly (2001a) for a range of
749 sedimentary compositions from Plank and Langmuir (1998) and Plank (2013).

750 The estimates of CO_2 loss in **Table 3** demonstrate the strong, expected relationship between
751 extents of deep volatiles cycling and subduction-zone thermal structure, the latter related to a
752 number of physical and thermal factors (see discussions of the more recent thermal models by
753 Syracuse et al., 2010; van Keken et al., 2011). For the closed-system model, extensive (perhaps
754 complete) CO_2 loss is expected to occur in carbonated basalt and the more mixed clastic-
755 carbonate sediment sections (for the latter, GLOSS and Antilles), whereas ophicarbonate and the
756 more pure carbonate sections (Marianas, Vanuatu) could retain large fractions of their CO_2 over
757 this depth range. Here, it is important to recall that subducting altered oceanic crust is believed to

convey one-half to two-thirds of the C entering trenches, on a global basis (see **Table 1**). The same metabasaltic composition (417A-24) could lose as little as 7% of its CO_2 traversing this same depth range in the very "cool" Tonga margin. It is unlikely that the endmember closed-system modeling truly approximates decarbonation history at depth in subduction zones, as the limited, evolving permeability of the intact volumes of rocks will afford some pervasive infiltration, and fracture networks are likely to greatly enhance access to the carbonate-bearing sections by H_2O-rich fluids derived elsewhere in the subducting sediment and ophiolitic section. Also uncertain is the role of partial melting of various subducting lithologies in mobilizing C beneath arcs (van Keken et al., 2011; Tsuno et al., 2012; discussion by Dasgupta, 2013). Thus, the estimates of CO_2 loss in **Table 3** provide a crude assessment of the *minimum* losses expected for such rocks.

An assessment of whether closed-system to limited open-system behavior, as demonstrated here, can result in decarbonation sufficient to balance arc CO_2 outputs is further complicated by the poor constraints on volcanic CO_2 flux in many individual arcs (see the review by Hilton et al., 2002). The most detailed attempt to match subduction C inputs with arc volcanic gas outputs was that of de Leeuw et al. (2007), who suggested that the contribution sediment-induced C alone could account for the measured output of gases and estimated a C return of 12-18% in Costa Rica and ~29% in El Salvador. The calculated CO_2 losses in **Table 3**, for subduction along moderately warm *P-T* paths such as those at the Central America margin (for Costa Rica and Columbia/El Salvador, very similar to the path for N. Vanuatu; van Keken et al., 2011), are consistent with the proposed CO_2 returns from subducting sediments in that margin (12-29%), depending on the exact proportions in that margin of mixed carbonate-clastic sediments undergoing reaction. Interestingly, a slightly larger return of CO_2 is estimated for the El Salvador

781 margin for which the *P-T* path is somewhat warmer than that for Costa Rica. However, de Leeuw
782 et al. (2007) provide a discussion of the full range of factors that could control these arc volcanic
783 returns.

784 In addition to decarbonation (and possibly, partial melting), carbonate dissolution, discussed
785 by Ague and Nicolescu (2014; see Manning, 2014; cf. John et al., 2008) and Facq et al. (2014),
786 and conceivably also carbonate reduction (Galvez et al., 2013; Lazar et al., 2014), could mobilize
787 C from slabs, particularly in regions experiencing significant fluid flux (more densely fractured
788 rock volumes, shear zones). Greater understanding of the significance of these processes in
789 contributing to C flux from subducting slab+sediment sections awaits further field and
790 geochemical investigation. Further confounding any quantitative assessment of C flux from these
791 sections, regardless of the mechanism, is the observation that C can also be *enriched/deposited* in
792 some sites, for example, in veins and their envelopes (as both carbonate and graphite; see Bebout,
793 1995; Gao et al., 2007; Beinlich et al., 2010). In this scenario, C is redistributed within
794 subducting slabs and evolving subduction interfaces, but not necessarily removed from these
795 domains and available for addition to the overlying mantle wedge. At shallower levels of
796 forearcs (<40 km), particularly in paleoaccretionary complexes, this C "capture" is demonstrated
797 by the voluminous carbonate veining and, to a lesser extent, deposition of graphite in veins (see
798 Bebout and Barton, 1993; Bebout, 1995; Sadofsky and Bebout, 2003).

799 A number of other factors can be envisioned as important in dictating C losses at individual
800 margins, beyond the varying thermal structures, types of sediments, and extents of carbonation in
801 subducting slabs on which we focus in this paper. The thickness of the upper lithospheric plate
802 dictates the depths at which the tops of subducting slabs are heated by exposure to the convecting
803 mantle wedge. Structural state of the incoming oceanic crustal section, and related degrees of

804 seafloor alteration, can be strongly affected by the rates of spreading, with oceanic crust
805 produced by slow spreading (e.g., Atlantic type) tending to be more hydrothermally altered and
806 with gabbros and ultramafic rocks exposed to seawater by large-scale extensional faulting. In the
807 Atlantic Ocean, hydrated and carbonated ultramafic rocks have been recovered by dredging and
808 are believed to be abundant on the modern seafloor (Cannat et al., 1997). Finally, modern
809 margins show varying degrees of subduction accretion and erosion (Scholl and von Huene, 2010),
810 in some cases varying along individual margins, and such processes could strongly influence (1)
811 the extent to which parts of the initially subducted sediment section are subducted into the deep
812 forearc and to beneath arcs, and (2) whether large amounts of C-bearing forearc material are
813 entrained to great depths by removal from the hanging wall.
814
815 **6. Conclusions and Outlook**
816 Following are some conclusions reached in this integrated field, petrologic, and geochemical
817 study and several comments regarding some directions that could be taken in further
818 investigation of metamorphic C fluxes in subduction zones.
819 — Combining our results with those of Cook-Kollars et al. (2014), it appears that intact volumes
820 of forearc-metamorphosed metabasaltic, meta-ultramafic, and metasedimentary rocks,
821 away from zones of more intense deformation (shear zones, dense fracture networks with
822 through-going veins), could experience only minor amounts of decarbonation, retaining
823 unreacted carbonate with varying textures during prograde metamorphism to depths
824 approaching those beneath volcanic fronts. In metabasalts, the majority of this carbonate
825 likely resides in interpillow regions and breccia matrices, as has been observed for altered
826 oceanic crust recovered during deep-sea drilling (see Gillis and Coogan, 2011). Loss of

827 CO_2 from ophicarbonates also appears minor based on combination of field results with
828 modeling and isotopic study.
829 — Rocks of these compositions could experience far larger amounts of decarbonation if
830 infiltrated by H_2O-rich fluids (consistent with the modeling results of Kerrick and
831 Connolly, 1998, 2001a,b; Connolly, 2005; Gorman et al., 2006). Taking into account the
832 effects of limited open-system behavior, and matching Perple_X calculations with
833 observed mineral modes, Cook-Kollars et al. (2014) estimated 10-20% loss of CO_2 from
834 the Schistes Lustres/Cignana metasedimentary section. Shifts in $\delta^{18}O$ in some
835 metabasalts, correlated with decrease in $\delta^{13}C$, and extremely uniform $\delta^{18}O$ in other suites,
836 could reflect infiltration by H_2O-rich fluids from external sources.
837 — Decarbonation, and also carbonate dissolution, is probably enhanced in shear zones and more
838 dense networks of larger-scale veins — the amount of such loss could be significant
839 along major pathways of slab fluid release or disrupted subduction interfaces at which
840 disparate lithologies are juxtaposed and experience interaction with large amounts of
841 fluid (see Bebout and Penniston-Dorland, 2014, in review). Further field-based work
842 should be aimed at assessing extents of loss of volatiles along such structures, the
843 mechanisms of loss (e.g., decarbonation, carbonate dissolution, in part related to fluid
844 influx or mixing; see John et al., 2008; Poli et al., 2009), and whether this loss can
845 contribute significantly to the overall C flux from subducting slab+sediment sections.
846 — Organic C is estimated as representing ~20% of the subduction C input inventory (Agrinier et
847 al., 1985; Bebout, 2007b). Although the delivery of this reduced C reservoir into
848 subduction zones is expected to be dominantly in sediments, there is some suggestion that
849 deeply subducting metabasaltic rocks could contain significant amounts of reduced C

(see **Section 4.2**) that should be considered in assessments of deep C subduction. Of the three whole-rock analyses of reduced C presented in this paper, two resemble organic C in their $\delta^{13}C$ (near -25‰), and the third resembles the upper mantle, near -5‰.

— The increased heating of subducting slabs and sediments over the approximate depth interval of 80-120 km (see the paths in **Figs. 6,8A,10**), related to exposure of the top-slab section to the convecting mantle wedge, could have profound significance for the deep subduction cycling of volatiles, including CO_2 and other C species (also see Cook-Kollars et al., 2014). This heating would enhance decarbonation and dissolution and potentially lead to partial melting (van Keken et al., 2011; Tsuno et al., 2012; discussion by Dasgupta, 2013), conceivably resulting in release of C in quantities sufficient to balance arc outputs.

— Return of slab-released C to the atmosphere in volcanic arc gases could be quite inefficient — large amounts of C could be stored in the forearc and in the subarc mantle wedge. Greater understanding of this storage is necessary for estimates of the proportion of initially subducted C entering the deeper mantle (i.e., surviving to depths beyond subarc regions).

— Our work points to the need to investigate C cycling at individual margins with well-known physical characteristics, including subduction inputs, and thermal structure. Such work might best be done on individual margins for which such parameters are known to vary along strike, providing an analysis of the most important forcing factors (see de Leeuw et al., 2007; House et al., 2014).

Acknowledgements

Funding for this project came mostly from National Science Foundation grant EAR-1119264 (to GEB). We extend special thanks to James Connolly for his helpful comments and assistance with the use of the Perple_X software, and to Peter van Keken for providing updated calculated *P-T* paths for modern subduction margins. Rosalind Coggon kindly provided a compilation of the O and C isotope compositions of veins in seafloor basalts. MS acknowledges funding from the Italian MIUR (PRIN-COFIN project 2012R33ECR_002).

References

Agard, P., Fournier, M., Lacombe, O., 2003. Post-nappe brittle extension in the inner Western Alps (Schistes Lustres) following late ductile exhumation: a record of synextension block rotation? Terra Nova 15, 306-314.

Agrinier, P., Javoy, M., Smith, D.C., Pineau, F., 1985. Carbon and oxygen isotopes in eclogites, amphibolites, veins and marbles from the Western Gneiss region, Norway. Chem. Geol. 52, 145-162.

Ague, J.J., Nicolescu, S., 2014. Carbon dioxide released from subduction zones by fluid-mediated reactions. Nature Geosci., DOI: 10.1038/NGEO2143.

Ague, J.J., Rye, D.M., 1999. Simple models of CO_2 release from metacarbonates with implications for interpretation of directions and magnitudes of fluid flow in the deep crust. Jour. Petrol. 40, 1443-1462.

Alt, J.C., 2004. 15. Alteration of the upper oceanic crust: mineralogy, chemistry, and processes. in Davis, E.E., Elderfield, H., Hydrogeology of the Oceanic Lithosphere, Cambridge University Press, pp. 497-535.

Alt, J.C., Laverne, C., Vanko, D.A., Tartarotti, P., Teagle, D.A., Bach, W., Wilkens, R.H., 1996. Hydrothermal alteration of a section of upper oceanic crust in the eastern equatorial Pacific: A synthesis of results from Site 504 (DSDP Legs 69, 70, and 83, and ODP Legs 111, 137, 140, and 148). Proc. Ocean Drill. Progr. Sci. Res., 417-434.

Alt, J.C., Schwarzenbach, E.M., Fruh-Green, G.L., Shanks III, W.C., Bernasconi, S.M., Garrido, C.J., Crispini, L., Gaggero, L., Padron-Navarta, J.A., Marchesi, C., 2013. The role of serpentinites in cycling of carbon and sulfur: Seafloor serpentinization and subduction metamorphism. Lithos 178, 40-54.

Alt, J.C., Teagle, D.A.H., 2003. Hydrothermal alteration of upper oceanic crust formed at a fast spreading ridge: mineral, chemical, and isotopic evidence from ODP Site 801. Chem. Geol. 201, 191-211.

Alt, J.C., Teagle, D.A.H., Laverne, C., Vanko, D., Bach, W., Honnorez, J., Becker, K., Ayadi, M., and Pezard, P.A., 1996. Ridge flank alteration of upper ocean crust in the eastern Pacific: a synthesis of results for volcanic rocks of holes 504B and 896A. In Proceedings of the Ocean Drilling Program, Scientific Results , Vol. 148, eds. J.C. Alt, H. Kinoshita, L.B. Stokking, and P.J. Michael. College Station, TX: Ocean Drilling Program, pp. 434–452.

Angiboust, S., Agard, P., 2010. Initial water budget: The key to detaching large volumes of eclogitized oceanic crust along the subduction channel? Lithos 120, 453-474.

909 Angiboust, S., Agard, P., Jolivet, L., Beyssac, O., 2009. The Zermatt–Saas ophiolite: the largest (60 km
910 wide) and deepest (c. 70–80 km) continuous slice of oceanic lithosphere detached from a subduction
911 zone? Terra Nova, 21, 171–180.

912 Angiboust, S., Agard, P., Raimbourg, H., Yamato, P., Huet, B., 2011. Subduction interface processes
913 recored by eclogite-facies shear zones (Monviso, W. Alps). Lithos 127, 222-238.

914 Angiboust, S., Langdon, R., Agard, P., Waters, D., Chopin, C., 2012. Eclogitization of the Monviso
915 ophiolite (W. Alps) and implications on subduction dynamics. Jour. Metamorphic Petrol. 30, 37-61.

916 Angiboust, S., Pettke, T., de Hoog, J.C.M., Caron, B., Oncken, O., 2014. Channelized fluid flow and
917 eclogite-facies metasomatism along the subduction shear zone. Jour. Petrol. 55, 883-916.

918 Artemyev, D.A., Zaykov, V.V., 2010. The types and genesis of ophicalcites in lower Devonian
919 olistostromes at cobalt-bearing massive sulfide deposits in the West Magnitogorsk paleoisland arc
920 (South Urals). Russ. Geol. Geophys. 51, 750–763.

921 Barbieri, M., Masi, U., Tolomeo, L., 1979. Stable isotope evidence for a marine origin of ophicalcites
922 from the north-central Apennines (Italy). Mar. Geol. 30, 193–204. doi:10.1016/0025-3227
923 (79)90015-X.

924 Barnicoat, A.C., Cartwright, I., 1995. Focused fluid flow during subduction: Oxygen isotope data from
925 high-pressure ophiolites of the western Alps. Earth Planet. Sci. Lett. 132, 53-61.

926 Barrett, T.J., Friedrichsen, H., 1989. Stable isotopic composition of atypical ophiolitic rocks from east
927 Liguria, Italy. Chem. Geol. Isot. Geosci. Sect. 80(1), 71–84. doi: 10.1016/0168-9622(89)90049-3.

928 Bebout, G.E., 1991a. Field-based evidence for devolatilization in subduction zones: implications for arc
929 magmatism. Science 251, 413-416.

930 Bebout, G.E., 1991b. Geometry and mechanisms of fluid flow at 15 to 45 kilometer depths in an early
931 Cretaceous accretionary complex. Geophys. Res. Lett. 18, 923-926.

932 Bebout, G.E., 1995. The impact of subduction-zone metamorphism on mantle-ocean chemical cycling.
933 Chem. Geol. 126, 191-218.

934 Bebout, G.E., 2007a. Metamorphic chemical geodynamics of subduction zones. Earth Planet. Sci. Lett.
935 260, 373-393.

936 Bebout, G.E., 2007b. Ch. 3.20. Trace element and isotopic fluxes/subducted slab, for Rudnick, R.L., ed.,
937 The Crust, Treatise on Geochemistry, Elsevier (eds. K. K. Turekian, H. D. Holland, and R. Rudnick),
938 doi:10.1016/B978-008043751-4/00231-5.

939 Bebout, G.E., 2013. Chapter 9. Metasomatism in subduction zones of subducted oceanic slabs, mantle
940 wedges, and the slab-mantle interface, in Harlov, D., and Austrheim, H., eds., Metasomatism and the
941 Chemical Transformation of Rock, The Role of Fluids in Terrestrial and Extraterrestrial Processes,
942 Springer-Verlag, pp. 289-349.

943 Bebout, G.E., 2014. 4.20. Chemical and isotopic cycling in subduction zones, in Rudnick, R. L., ed., The
944 Crust, Treatise on Geochemistry (eds. H. D. Holland and K. K. Turekian, Second Edition), Elsevier-
945 Pergamon, Oxford, pp. 703-747.

946 Bebout, G.E., Agard, P., Kobayashi, K., Moriguti, T., Nakamura, E., 2013. Devolatilization history, and
947 related trace element mobility, in deeply subducted sedimentary rocks: SIMS evidence from Western
948 Alps HP/UHP suites. Chem. Geol. 342, 1-20.

949 Bebout, G.E., Barton, M.D., 1993. Metasomatism during subduction: products and possible paths in the
950 Catalina Schist, California. Chem. Geol. 108, 61-92.

951 Bebout, G.E., Fogel, M.L., 1992. Nitrogen-isotope compositions of metasedimentary rocks in the Catalina,
952 California - Implications for metamorphic devolatilization history. Geochim. Cosmochim. Acta 56,
953 2839-2849.

954 Bebout, G.E., Nakamura, E., 2003. Record in metamorphic tourmalines of subduction zone
955 devolatilization and boron cycling. Geology 31, 407-410.

956 Bebout, G.E., Penniston-Dorland, S.C., 2014. Deformation and metasomatic evolution of the subduction
957 plate interface as viewed from study of HP and UHP metamorphic rocks (abstract). Fall Meeting,
958 American Geophysical Union, San Francisco, December, 2014.

959 Bebout, G.E., Penniston-Dorland, S.C., in review. Deformation-enhanced fluid and mass transfer at the
960 subduction plate interface, submitted to Lithos.

961 Becker, H., Altherr, R., 1992. Evidence from ultra-high pressure marbles for recycling of sediments into
962 the mantle. Nature 358, 745-748.

963 Beinlich, A., Klemd, R., John, T., and Gao, J., 2010, Trace-element mobilization during Ca-
964 metasomatism along a major fluid conduit: Eclogitization of blueschist as a consequence of fluid–
965 rock interaction. Geochim. Cosmochim. Acta 74, 1892-1922.

966 Berner, R.A., 1999. A new look at the long-term carbon cycle. GSA Today 9, 1-6.

967 Berner, R.A., Lasaga, A.C., Garrels, R.M., 1983. The carbonate-silicate geochemical cycle and its effect
968 on atmospheric carbon dioxide over the past 100 million years. Amer. Jour. Sci. 283, 641-683.

969 Breeding, C.M., Ague, J.J., Brocker, M., 2004. Fluid-metasedimentary interactions in subduction
970 zone mélange: implications for the chemical composition of arc magmas. Geology 32, 1041-1044.

971 Brotzu, P., Ferrini, V., Masi, U., Morbidelli, L., Turi, B., 1973. Contributo alla conoscenza delle «Rocce
972 Verdi» dell'Appennino centrale. Nota III. La composizione isotopica della calcite presente in alcuni
973 affioramenti di oficalciti del F 129 (S. Fiora) e sue implicazioni petrologiche. Period. Mineral. 42,
974 591–619.

975 Busigny, V., Cartigny, P., Philippot, P., Ader, M., Javoy, M., 2003. Massive recycling of nitrogen and
976 other fluid-mobile elements (K, Rb, Cs, H) in a cold slab environment: evidence from HP to UHP
977 oceanic metasediments of the Schistes Lustres nappe (western Alps, Europe). Earth Planet. Sci. Lett.
978 215, 27-42.

979 Cannat, M., Lagabrielle, Y., Bougault, H., Casey, J., De Coutures, N., Dmitriev, L., 1997. Ultramafic and
980 gabbroic exposures at the Mid-Atlantic ridge: geological mapping in the 151N region. Tectonophys.
981 279, 197–213.

982 Cartwright, I., Barnicoat, A.C., 1999. Stable isotope geochemistry of Alpine ophiolites: a window to
983 ocean-floor hydrothermal alteration and constraints on fluid-rock interaction during high-pressure
984 metamorphism. Int. J. Earth Sci. 88, 219-235.

985 Cartwright, I. Barnicoat, A.C., 2003. Geochemical and stable isotope resetting in shear zones from
986 Taschalp: constraints on fluid flow during exhumation in the Western Alps. Jour. Metamorphic Geol.
987 21, 143-161.

988 Castelli, D., Rolfo, F., Groppo, C., Compagnoni, R., 2007. Impure marbles from the UHP Brossasco-
989 Isasca Unit (Dora-Maira Massif, western Alps): evidence for Alpine equilibration in the diamond
990 stability field and evaluation of the X(CO_2) fluid evolution. Jour. Metamorphic Geol. 25, 587-603.

991 Clerc, C., Boulvais, P., Lagabrielle, Y., de Saint Blanquat, M., 2014. Ophicalcites from the northern
992 Pyrenean belt: a field, petrographic and stable isotope study. Int. J. Earth Sci. 103(1), 141-163.

Coggan, R.M., Teagle, D.A.H., Smith-Duque, C.E., Alt, J.C., Cooper, M.J., 2010. Reconstructing past seawater Mg/Ca and Sr/Ca from mid-ocean ridge flank calcium carbonate veins. Science 327, 1114-1117.

Connolly, J.A.D., 2005. Computation of phase equilibria by linear programming: a tool for geodynamic modeling and its application to subduction zone decarbonation. Earth Planet. Sci. Lett. 236, 524-541.

Cook-Kollars, J., Bebout, G.E., Collins, N.C., Angiboust, S., Agard, P., 2014. Subduction zone metamorphic pathway for deep carbon cycling: Evidence from HP/UHP metasedimentary rocks, Italian Alps. Chem. Geol., doi: 10.1016/j.chemgeo.2014.07.013.

Dasgupta, R., 2013. Ingassing, storage, and outgassing of terrestrial carbon through geologic time. Rev. Mineral. Geochem. 75, 183-229.

Dasgupta, R., Hirschmann, M.M., 2010. The deep carbon cycle and melting in Earth's interior. Earth Planet. Sci. Lett. 298, 1-13.

de Leeuw, G.A.M., Hilton, D.R., Fischer, T.P., Walker, J.A., 2007. The He-CO_2 isotope and relative abundance characteristics of geothermal fluids in El Salvador and Honduras: New constraints on volatile mass balance of the Central American Volcanic Arc. Earth Planet. Sci. Lett. 258, 132-146.

Demeny, A., Vennemann, T., Koller, F., 2007. Stable isotope compositions of the Penninic ophiolites of the Köszeg-Rechnitz series. Central. Eur. Geol. 50(1), 29–46, doi:10.1556/CEuGeol.50.2007.1.3.

Desmons, J., Aprahamian, J., Compagnoni, R., Cortesogno, L., Frey, M., 1999a. Alpine metamorphism of the Western Alps: I. Middle to high T/P metamorphism. Schweiz. Mineral. Petrogr. Mitt. 79, 89–110.

Desmons, J., Aprahamian, J., Compagnoni, R., Cortesogno, L., Frey, M., 1999b. Alpine metamorphism of the Western Alps: II. High P/T and related pre-greenschist metamorphism. Schweiz. Mineral. Petrogr. Mitt. 79, 111-134.

Evans, C.A., Baltuck, M., 1988. Low-temperature alteration of peridotite, hole 637A. In: Boillot G, Winterer EL et al (ed.) Proc. Ocean Drill. Progr. Sci. Res., 103, 235–239, http://www.odp.tamu.edu/publications/103_SR/103TOC.HTML.

Facq, S., Daniel, I., Montagnac, G., Cardon, H., Sverjensky, D.A., 2014. *In situ* Raman study and thermodynamic model of aqueous carbonate speciation in equilibrium with aragonite under subduction zone conditions. Geochim. Cosmochim. Acta 132, 375-390.

Frezzotti, M.L., Huizenga, J.M., Compagnoni, R., Selverstone, J., 2014. Diamond formation by carbon saturation in C-O-H fluids during cold subduction of oceanic lithosphere. Geochim. Cosmochim. Acta, http://dx.doi.org/10.1016/j.gca.2013.12.022.

Frezzotti, M.L., Selverstone, J., Sharp, Z.D., Compagnoni, R., 2011. Carbonate dissolution during subduction revealed by diamond-bearing rocks from the Alps. Nature Geosci. 4, 703-706.

Furnes, H., Muehlenbachs, K., Torsvik, T., Thorseth, I.H., Tumyr, O., 2001. Microbial fractionation of carbon isotopes in altered basaltic glass from the Atlantic Ocean, Lau Basin and Costa Rica Rift. Chem. Geol. 173, 313-330.

Fusseis, F., Regenauer-Lieb, K., Liu, J., Hough, R.M., De Carlo, F., 2009. Creep cavitation can establish a dynamic granular fluid pump in ductile shear zones. Nature 459, 974-977.

Galvez, M.E., Beyssac, O., Martinez, I., Benzerara, K., Chaduteau, C., Malvoisin, B., Malavielle, J., 2013. Graphite formation by carbonate reduction during subduction. Nature Geosci., DOI: 10.1038/NGEO1827.

Gao, J., John, T., Klemd, R., Xiong X., 2007. Mobilization of Ti–Nb–Ta during subduction: evidence from rutile-bearing dehydration segregations and veins hosted in eclogite, Tianshan, NW China. Geochim. Cosmochim. Acta 71, 4974–4996.

Gao, J., Klemd, R., 2003. Formation of HP-LT rocks and their tectonic implications in the western Tianshan Orogen, NW China; geochemical and age constraints. Lithos 66, 1-22.

Gasparik, T., 1989. Experimental study of subsolidus phase relations and mixing properties of pyroxene and plagioclase in the system Na_2O-CaO-Al_2O_3-SiO_2, Contrib. Mineral. Petrol. 89 346-357.

Gebauer, D., Schertl, H.-P., Brix, M., Schreyer, W., 1997. 35 Ma old ultrahigh-pressure metamorphism and evidence for very rapid exhumation in the Dora Maira massif, Western Alps. Lithos 41, 5–24.

Gillis, K.M., Coogan, L.A., 2011. Secular variation in carbon uptake into the oceanic crust. Earth Planet. Sci. Lett. 302, 385-392.

Gorman, P.J., Kerrick, D.M., Connolly, J.A.D., 2006. Modeling open system metamorphic decarbonation of subducting slabs. Geochem. Geophys. Geosyst. 7, Q04007, doi:10.1029/2005GC001125.

Groppo, C., Beltrando, M., Compagnoni, R., 2009. The P-T path of the ultra-high pressure Lago di Cignana and adjoining high-pressure meta-ophiolitic units: insights into the evolution of the subducting Tethyan slab. Jour. Metamorphic Geol. 27, 207-231.

Halldorsson, S.A., Hilton, D.R., Troll, V.R., Fischer, T.P., 2013. Resolving volatile sources along the western Sunda arc, Indonesia. Chem. Geol. 339, 263-282.

Herms, P., John, T., Bakker, R.J., Schenk, V., 2012. Evidence for channelized external fluid flow and element transfer in subducting slabs (Raspas Complex, Ecuador). Chem. Geol. 310-311, 79-96.

Hilton, D.R., Fischer, T.P., Marty, B., 2002. Noble gases and volatile recycling at subduction zones. Rev. Mineral. Geochem. 47, 319.

Holland, T., Powell, R., 1991. A Compensated-Redlich-Kwong (CORK) equation for volumes and fugacities of CO_2 and H_2O in the range 1 bar to 50 kbar and 100–1600 ˚C. Contrib. Mineral. Petrol. 109, 265-273.

Holland, T.J.B., Powell, R., 1998. An internally consistent thermodynamic data set for phases of petrological interest. Jour. Metamorphic Geol. 16, 309-343.

House, B.M., Bebout, G.E., Hilton, D.R., Rodriguez, B., Plank, T., 2014. Constraining sources of subducted and recycled carbon along the Sunda Arc (abstract), Amer. Geophys. Un. Ann. Meeting, San Francisco, December, 2014.

Jarrard, R.D., 2003. Subduction fluxes of water, carbon dioxide, chlorine, and potassium. Geochem. Geophys. Geosyst. 5; doi:10.1029/2002GC000392.

Javoy, M.,1998. The birth of the Earth's atmosphere: the behaviour and fate of its major elements. Chem. Geol. 147, 11-25.

Jedrysek, M.O., Weber-Weller, A., Szynkiewicz, A., Mierzejewski, M., 2000, Evolution of Sleza and Nowa Ruda Ophiolites: Oceanic and Continental Stages Recorded in Stable Isotope Composition of Oxides, Carbonates and Sulphides. GeoLines (Praha) 10.

Joesten, R., 1977. Evolution of mineral assemblage zoning in diffusion metasomatism. Geochim. Cosmochim. Acta 41, 649-670.

John, T., Gussone, N., Podladchikov, Y.Y., Bebout, G.E., Dohmen, R., Halama, R., Klemd, R., Magna, T., Seitz, H.M., 2012. Volcanic arcs fed by rapid pulsed fluid flow through subducting slabs, Nature Geosci. 5, 489-492.

John, T., Klemd, R., Gao, J., Garbe-Schonberg, C.D., 2008, Trace-element mobilization in slabs due to non steady-state fluid-rock interaction: constraints from an eclogite-facies transport vein in blueschist (Tianshan, China). Lithos 103, 1-24.

John, T., Schenk, V., 2003. Partial eclogitisation of gabbroic rocks in a late Precambrian subduction zone (Zambia): prograde metamorphism triggered by fluid infiltration. Contrib. Mineral. Petrol. 146, 174-191.

Jolivet, L., Faccena, C., Goffe, B., Burov, E., Agard, P., 2003. Subduction tectonics and exhumation of high-pressure metamorphic rocks in the Mediterranean orogens. Amer. Jour. Sci. 303, 353-409.

Kato, T., Enami, M. Zhai, M., 1997. Ultra-high-pressure (UHP) marble and eclogite in the Su-Lu UHP terrane, eastern China. Jour. Metamorphic Geol. 15, 169–182.

Kerrick, D.M., 2001. Present and past nonanthropogenic CO_2 degassing from the solid Earth. Rev. Geophys. 39, 565-585.

Kerrick, D.M., Connolly, J.A.D., 1998. Subduction of ophicarbonates and recycling of CO_2 and H_2O. Geology 26, 375-378.

Kerrick, D.M., Connolly, J.A.D., 2001a. Metamorphic devolatilization of subducted marine sediments and the transport of volatiles into the Earth's mantle. Nature 411, 293-296.

Kerrick, D.M., Connolly, J.A.D., 2001b. Metamorphic devolatilization of subducted oceanic metabasalts: implications for seismicity, arc magmatism and volatile recycling. Earth Planet. Sci. Lett. 189, 19-29.

King, R.L., Bebout, G.E., Grove, M., Moriguti, T., Nakamura, E., 2007. Boron and lead isotope signatures of subduction-zone melange formation: Hybridization and fractionation along the slab-mantle interface beneath volcanic arcs. Chem. Geol. 239, 305-322.

King, R.L., Bebout, G.E., Kobayashi, K., Nakamura, E., van der Klauw, S.N.G.C., 2004. Ultrahigh-pressure metabasaltic garnets as probes into deep subduction zone chemical cycling. Geochem. Geophys. Geosyst., Q12J14, doi:10.1029/2004GC000746.

King, R.L., Bebout, G.E., Moriguti, T., Nakamura, E., 2006. Elemental mixing systematics and Sr-Nd isotope geochemistry of mélange formation: Obstacles to identification of fluid sources to arc volcanics. Earth Planet. Sci. Lett. 246, 288-304.

Klemd, R., Schroter, F.C., Will, T.M. Gao, J., 2002. P-T evolution of glaucophane-omphacite bearing HP-LT rocks in the western Tianshan Orogen, NW China; new evidence for "Alpine-type" tectonics. Jour. Metamorphic Geol. 20, 239-254.

Klemd, R., Brocker, M., Hacker, B.R., Gao, J., Gans, P., Wemmer, K., 2005. New age constraints on the metamorphic evolution of the high-pressure/low-temperature belt in the western Tianshan Mountains, NW China. Jour. Geol. 113, 157-168.

Klemd, R., John, T., Scherer, E.E., Rondenay, S., Gao, J., 2011. Changes in dip of subducted slabs at depth: Petrological and geochronological evidence from HP-UHP rocks (Tianshan, NW-China). Earth Planet. Sci. Lett., 310, 9-20.

Konrad-Schmolke, M., Halama, R., 2014. Combined thermodynamic-geochemical modeling in metamorphic geology: Boron as tracer of fluid-rock interaction. Lithos 208-209, 393-414.

Lagabrielle, Y., Cannat, M., 1990. Alpine Jurassic ophiolites resemble the modern central Atlantic basement. Geology 18, 319-322.

Lavoie, D., Cousineau, P.A., 1995. Ordovician ophicalcites of southern Quebec Appalachians: a proposed early seafloor tectonosedimentary and hydrothermal origin. Jour. Sediment. Res. 65(2a), 337–347.

Lazar, C., Zhang, C., Manning, C.E., Mysen, B.O., 2014. Redox effects on calcite-portlandite-fluid equilibria at forearc conditions: Carbon mobility, methanogenesis, and reduction melting of calcite. Amer. Mineral. 99, 1604-1615.

Leoni, L., Marroni, M., Sartori, F., Tamponi, M., 1996. Metamorphic grade in metapelites of the internal liguride units (Northern Apennines, Italy). Eur. J. Min. 8(1), 35-50.

Li, L., Bebout, G.E., 2005. Carbon and nitrogen geochemistry of sediments in the Central American convergent margin: Insights regarding subduction input fluxes, diagenesis, and paleoproductivity. Jour. Geophys. Res. 110, B11202.

Lu, Z., Zhang, L., Chen, Z., 2014. Jadeite- and dolomite-bearing coesite eclogite from western Tianshan, NW China. Eur. J. Mineral. 26, 245-256.

Manning, C.E., 2014. A piece of the deep carbon puzzle (News & Views). Nature Geosci., April 20, 2014.

Marin-Ceron, M.I., Moriguti, T., Makishima, A., Nakamura, E., 2010. Slab decarbonation and CO_2 recycling in the Southwestern Colombian volcanic arc. Geochim. Cosmochim. Acta 74, 1104-1121.

Martin, S., Rebay, G., Kienast, J.-R., Mevel, C., 2008. An eclogitised oceanic paleohydrothermal field from the St. Marcel Valley (Italian Western Alps). Ofioliti 33, 49-63.

Martin, S., Tartarotti, P., 1989. Polyphase HP Metamorphism in the ophiolitic gaucophanites of the Lower St. Marcel Valley (Aosta, Italy). Ofioliti 14. 135–156.

Marty, B., Tolstikhin, I.N., 1998. CO_2 fluxes from mid-ocean ridges, arcs and plumes. Chem. Geol. 145, 233-248.

Michard, A., Avigad, D., Goffe, B., Chopin, C., 2004. The high-pressure metamorphic front of the south Western Alps (Ubaye-Maira transect, France, Italy). Schweiz. Mineral. Petrogr. Mitt. 84, 215-235.

Miller, J.A., Cartwright, I., 2000. Distinguishing between seafloor alteration and fluid flow during subduction using stable isotope geochemistry: examples from Tethyan ophiolites in the Western Alps. Jour. Metamorphic Geol. 8, 467-482.

Miller, J.A., Cartwright, I., Buick, I.S. Barnicoat, A.C., 2001. An O-isotope profile through the HP-LT Corsican ophiolite, France and its implications for fluid flow during subduction. Chem. Geol. 178, 43-69.

Miller, D.P., Marschall, H.R., Schumacher, J.C., 2009. Metasomatic formation and petrology of blueschist-facies hybrid rocks from Syros (Greece): Implications for reactions at the slab-mantle interface, Lithos 107, 53-67.

Milliken, K.L., Morgan, J.K., 1996. Chemical evidence for near-seafloor precipitation of cacite in serpentinites (site 897) and Serpentinite Breccias (Site 899), Iberia Abyssal Plain. In: Whitmarsh RB, Sawyer DS, Klaus A, Masson DG (eds) Proceedings of the ocean drilling program, 149 scientific results, vol. 149, Ocean Drilling Program, pp. 553–558, http://www-odp.tamu.edu/publications/149_SR/149TOC.HTML

Molina, J. F., and Poli, S., 2000. Carbonate stability and fluid composition in subducted oceanic crust: an experimental study on H_2O-CO_2-bearing basalts. Earth Planet. Sci. Lett. 176, 295-310.

Nadeau, S., Philippot, P. Pineau, F., 1993. Fluid inclusion and mineral isotopic compositions (H-C-O) in eclogitic rocks as tracers of local fluid migration during high-pressure metamorphism. Earth Planet. Sci. Lett. 114, 431-448.

Parrish, R.R., Gough, S.J., Searle, M.P., Waters, D.J., 2006. Plate velocity exhumation of ultra-high pressure eclogites in the Pakistan Himalaya. Geology 34, 989–992.

1160 Pelletier, L., Muntener, O., Kalt, A., Vennemann, T.W., Belgya, T., 2008. Emplacement of ultramafic
1161 rocks into the continental crust monitored by light and other trace elements: An example from the
1162 Geisspfad body (Swiss-Italian Alps). Chem. Geol. 255, 143-159.

1163 Philippot, P., 1993. Fluid-melt-rock interaction in mafic eclogites and coesite-bearing metasediments:
1164 constraints on volatile.recycling during subduction. In: J.L.R. Touret and A.B. Thompson (Guest-
1165 Editors), Fluid-Rock Interaction in the Deeper Continental Litbosphl:re. Chem. Geol. 108, 93-112
1166 (special issue).

1167 Philippot, P., Selverstone, J., 1991. Trace element-rich brines in eclogitic veins: implications for fluid
1168 composition and transport during subduction. Contrib. Mineral. Petrol. 106, 417–430.

1169 Plas, A., 1997. Petrologic and stable isotope constraints on fluid-rock interaction, serpentinization and
1170 alteration of oceanic ultramafic rocks. PhD Thesis, Swiss Federal Institute of Technology, Swiss.

1171 Plank T., 2014, 4.19. The chemical composition of subducting sediments, in Rudnick, R.L. (Ed.), The
1172 Crust, Treat. Geochem., 2nd edition, v. 4, Elsevier.

1173 Plank, T., Langmuir, C.H., 1998. The chemical composition of subducting sediment and its consequences
1174 for the crust and mantle. Chem. Geol. 145, 325-394.

1175 Platt, J.P., 1986. Dynamics of orogenic wedges and the uplift of high-pressure metamorphic rocks. Geol.
1176 Soc. Amer. Bull. 97, 1037-1053.

1177 Poli, S., Franzolin, E., Fumagalli, P., Crottini, A., 2009. The transport of carbon and hydrogen in
1178 subducted oceanic crust: An experimental study to 5 GPa. Earth Planet. Sci. Lett. 278, 350-360.

1179 Proyer, A., 2003. Metamorphism of pelites in NKFMASH – a new petrogenetic grid with implications for
1180 the preservation of high-pressure mineral assemblages during exhumation. Jour. Metamorphic Geol.
1181 21, 493-509.

1182 Proyer, A., Rolfo, F., Castelli, D., Compagnoni, R., 2014. Diffusion-controlled metamorphic reaction
1183 textures in an ultrahigh-pressure impure calcite marble from Dabie Shan, China. Eur. J. Mineral. 26,
1184 25-40.

1185 Ranero, C.R., Villasenor, A., Phipps Morgan, J., Weinrebe, W., 2005. Relationship between bend-faulting
1186 at trenches and intermediate-depth seismicity. Geochem. Geophys. Geosyst. 6, Q12002,
1187 doi:10.1029/2005GC000997.

1188 Reinecke, T., 1991. Very-high-pressure metamorphism and uplift of coesite-bearing metasediments from
1189 the Zermatt–Saas zone, Western Alps. Eur. J. Mineral. 3, 7–17.

1190 Reinecke, T., 1998. Prograde high- to ultrahigh-pressure metamorphism and exhumation of oceanic
1191 sediments at Lago di Cignana, Zermatt-Saas Zone, western Alps. Lithos 42, 147-189.

1192 Rubatto, D., Gebauer, D., Fanning, M., 1998. Jurassic formation and Eocene subduction of the Zermatt-
1193 Saas-Fee ophiolites: implications for the geodynamic evolution of the Central and Western Alps.
1194 Contrib. Mineral. Petrol. 132, 269-287.

1195 Rubatto, D., Hermann, J., 2001. Exhumation as fast as subduction? Geology 29, 3–6.

1196 Rubatto, D., Hermann, J., 2003. Zircon formation during fluid circulation in eclogites (Monviso, Western
1197 Alps): implications for Zr and Hf budget in subduction zones. Geochim. Cosmochim. Acta 67, 2173-
1198 2187.

1199 Sadofsky, S.J., Bebout, G.E., 2003. Record of forearc devolatilization in low-T, high-P/T
1200 metasedimentary suites: significance for models of convergent margin chemical cycling, Geochem.
1201 Geophy. Geosyst. 4, 9003, doi:10.1029/2002GC000412.

1202 Sano, Y., Williams, S.N., 1996. Fluxes of mantle subducted carbon along convergent margins. Geophys.
1203 Res. Lett. 23, 2749-2752.

1204 Sano, Y., Takahata, N., Nishio, Y., Fischer, T.P., Williams, S.N., 2001. Volcanic flux of nitrogen from
1205 the Earth. Chem. Geol. 171, 263-271.

1206 Scambelluri, M., Malaspina, N., Hermann, J., 2007. Subduction fluids and their interaction with the
1207 mantle wedge: a perspective from the study of high-pressure ultramafic rocks. Periodico di
1208 Mineralogia 76, 253-265.

1209 Scambelluri, M., Muntener, O., Ottolini, L., Pettke, T., Vannucci, R., 2004. The fate of B, Cl, and Li in
1210 the subducted oceanic mantle and in the antigorite breakdown fluids. Earth Planet. Sci. Lett. 222,
1211 217-234.

1212 Scambelluri, M., Philippot, P., 2001. Deep fluids in subduction zones. Lithos 55, 213-227.

1213 Schmidt, M.W., Poli, S., 2014. 4.19. Devolatilization during subduction, in Rudnick, R. L., ed., The Crust,
1214 Treatise on Geochemistry (eds. H. D. Holland and K. K. Turekian, Second Edition), Elsevier-
1215 Pergamon, Oxford, pp. 669-701.

1216 Scholl, D.W., von Huene, R., 2010. Subduction zone recycling processes and the rock record of crustal
1217 suture zones. Can. Jour. Earth Sci. 47, 633-654.

1218 Schwarzenbach, E.M., Fruh-Green, G.L., Bernasconi, S.M., Alt, J.C., Plas, A., 2013. Serpentinization and
1219 carbon sequestration: A study of two ancient peridotite-hosted hydrothermal systems. Chem. Geol.
1220 351, 115-133.

1221 Shaw, A.M., Hilton, D.R., Fischer, T.P., Walker, J.A., Alvarado, G.E., 2003. Contrasting He–C
1222 relationships in Nicaragua and Costa Rica: insights into C cycling through subduction zones. Earth
1223 Planet. Sci. Lett. 214, 499–513.

1224 Sheppard, S.M.F., Schwarcz, H.P., 1970. Fractionation of carbon and oxygen isotopes and magnesium
1225 between coexisting metamorphic calcite and dolomite. Contrib. Mineral. Petrol. 26, 161-198.

1226 Skelton, A.D., Valley, J.W., 2000. The relative timing of serpentinisation and mantle exhumation at the
1227 ocean-continent transition, Iberia: constraints from oxygen isotopes. Earth. Planet. Sci. Lett. 178,
1228 327–338.

1229 Spandler, C., Hermann, J., 2006. High-pressure veins in eclogite from New Caledonia and their
1230 significance for fluid migration in subduction zones. Lithos 89, 135-153.

1231 Spandler, C., Pettke, T., Rubatto, D., 2011. Internal and external fluid sources for eclogite-facies veins in
1232 the Monviso meta-ophiolite, Western Alps: Implications for fluid flow in subduction zones. Jour.
1233 Petrol. 52, 1207-1236.

1234 Staudigel, H., Hart, S.R., Schmincke, H.U., Smith, B.M., 1989. Cretaceous ocean crust at DSDP Sites 417
1235 and 418: Carbon uptake from weathering versus loss by magmatic outgassing. Geochim. Cosmochim.
1236 Acta 53, 3091-3094.

1237 Staudigel, H., Plank, T., White, B., Schmincke, H.U., 1996. Geochemical fluxes during seafloor alteration
1238 of the basaltic upper oceanic crust: DSDP Sites 417 and 418. in Bebout, G.E., Scholl, D.W., Kirby,
1239 S.H., Platt, J.P., eds., Subduction Top to Bottom, Amer. Geophys. Un. Geophys. Monogr. 96, 19-38.

1240 Syracuse, E.M., Abers, G.A., 2006. Global compilation of variations in slab depth beneath arc volcanoes
1241 and implications. Geochem. Geophys. Geosyst. Q05017, doi:10.1029/2005GC001045.

1242 Syracuse, E.M., van Keken, P.E., Abers, G.A., 2010. The global range of subduction zone thermal models.
1243 Phys. Earth Planet. Int. 183, 73-90.

Thompson, A. B., 1975. Calc-silicate diffusion zones between marble and pelitic schist. Jour. Petrol. 16, 314-346.

Tricart, P., Lemoine, M., 1986. From faulted blocks to megamullions and megaboudins: Tethyan heritage in the structure of the Western Alps. Tectonics 5, 95-118.

Tricart, P., Lemoine, M., 1991. The Queyras ophiolite west of Monte Viso (Western Alps): indicator of a peculiar ocean floor in the Mesozoic Tethys. Jour. Geodynam. 13, 163-181.

Tsuno, K., Dasgupta, R., 2011. Melting phase relation of nominally anhydrous, carbonated pelitic-eclogite at 2.5-3.0 GPa and deep cycling of sedimentary carbon. Contrib. Mineral. Petrol. 161, 743-763.

Tsuno, K., Dasgupta, R., Danielson, L., Righter, K., 2012. Flux of carbonate melt from deeply subducted pelitic sediments: Geophysical and geochemical implications for the source of Central American volcanic arc. Geophys. Res. Lett. 39, doi:10.1029/2012GL052606.

Valley, J.W., 1986. Stable isotope geochemistry of metamorphic rocks. Rev. Mineral. Geochem. 16, 445-489.

Vallis, F., Scambelluri, M., 1996. Redistribution of high-pressure fluids during retrograde metamorphism of eclogite-facies rocks (Voltri Massif, Italian Western Alps). Lithos 39, 81-92.

van der Meer, D.G., Zeebe, R.E., van Hinsbergen, D.J.J., Sluijs, A., Spakman, W., Torsvik, T.H., 2014. Plate tectonic controls on atmospheric CO_2 levels since the Triassic. Proc. National Acad. Sci. 111, 4380-4385.

van der Klauw, S.N.G.C., Reinecke, T., Stockhert, B., 1997. Exhumation of ultrahigh-pressure metamorphic oceanic crust from Lago di Cignana, Piemontese zone, western Alps: the structural record in metabasites. Lithos 41, 79-102.

van der Straaten, F., Schenk, V., John, T., Gao, J., 2008. Blueschist-facies rehydration of eclogites (Tian Shan, NW-China): Implications for fluid-rock interaction in the subducted channel. Chem. Geol. 255, 195-219.

van der Straaten, F., Halama, R., John, T., Schenk, V., Hauff, F., Andersen, N., 2012. Tracing the effects of high-pressure metasomatic fluids and seawater alteration in blueschist-facies overprinted eclogites: Implications for subduction channel processes. Chem. Geol. 292, 69-87.

van Keken, P.E., Hacker, B.R., Syracuse, E.M., Abers, G.A., 2011. Subduction factory: 4. Depth-dependent flux of H_2O from subducting slabs worldwide. Jour. Geophys. Res. 116, B01401, doi:10.1029/2010JB007922.

Vignaroli, G., Rossetti, F., Bouybaouene, M., Massonne J., Theye, T., Faccenna, C., and Funiciello, R., 2005, A counter-clockwise P–T path for the Voltri Massif eclogites (Ligurian Alps, Italy). Jour. Metamorphic Geol. 23, 533-555.

Wei, C., Powell, R., 2003. Phase relations in high-pressure metapelites in the system KFMASH (K_2O-FeO-MgO-Al_2O_3-SiO_2-H_2O) with application to natural rocks. Contrib. Mineral. Petrol. 145, 301-315.

Wei, C., Powell, R., Zhang, L., 2003. Eclogites from the south Tianshan, NW China: petrological characteristic and calculated mineral equilibria in the Na_2O-CaO-FeO $MgOAl_2O_3$-SiO_2-H_2O system. Jour. Metamorphic Geol. 21, 163-179.

Weissert, H., Bernoulli, D., 1984. Oxygen isotope composition of calcite in Alpine ophicarbonates: a hydrothermal or Alpine metamorphic signal? Eclogae. Geol. Helv. 77(1), 29–43.

Whitney, D.L., Evans, B.W., 2010. Abbreviations for names of rock-forming minerals. Amer. Mineral. 95(1), 185.

1287 Widmer, T., Thompson, A.B., 2001. Local origin of high pressure vein material in eclogite facies rocks of
1288 the Zermatt-Saas Zone, Switzerland. Amer. Jour. Sci. 301, 627-656.

1289 Zack, T., John, T., 2007. An evaluation of reactive fluid flow and trace element mobility in
1290 subducting slabs. Chem. Geol. 239, 199-216.

1291 Zhang, Y., Zindler, A., 1993. Distribution and evolution of carbon and nitrogen in Earth. Earth Planet.
1292 Sci. Lett. 117(3), 331-345.

1293 Zheng, Y.-F., 1993. Calculation of oxygen isotope fractionation in anhydrous silicate minerals. Geochim.
1294 Cosmochim. Acta 57, 1079-1091.

1295 Zheng, Y.-F., 2012. Metamorphic chemical geodynamics in continental subduction zones. Chem. Geol.
1296 328, 5-48, doi:10.1016/j.chemgeo.2012.02.005.

1297 Zheng, Y.-F., Fu, B., Gong, B., Li, L., 2003. Stable isotope geochemistry of ultrahigh pressure
1298 metamorphic rocks from the Dabie-Sulu orogen in China: implications for geodynamics and fluid
1299 regime. Ear.-Sci. Rev. 62, 105-161.

1300 Zimmer, M.M., Fischer, T.P., Hilton, D.R., Alvarado, G.E., Sharp, Z.D., Walker, J.A., 2004. Nitrogen
1301 systematics and gas fluxes of subduction zones: Insights from Costa Rica arc volatiles. Geochem.
1302 Geophy. Geosyst. 5, Q05J11, doi:10.1029/2003GC000651.

Figure Captions

Figure 1. (**A**) Generalized geologic map for the Western Alps detailing sample locations. See **Supplementary Table 1** for coordinates of sampling locations. (**B**) Pressure-temperature diagram showing peak *P-T* for the field localities and the *P-T* gradient defined by these units. *P-T* estimates for these locations are from Leoni et al. (1996), Michard et al. (2004), Angiboust et al. (2012), Vignaroli et al. (2005), Angiboust and Agard (2010), Groppo et al. (2009), and Frezzotti et al. (2011, 2014). Units for Monviso are denoted with LS for the Lago Superiore Unit and MV for the Monviso Unit.

Figure 2: Field photographs of pillow basalts with representative textures, all but (**C**) with a 35mm camera lens for scale. (**A**) Undeformeed prenhite-pumpellyite facies pillow basalts from the Bracco Unit. (**B**) Eclogite facies pillow basalt from the Lago Superiore Unit at Monviso. (**C**) Deformed meta-pillow basalts at the Lago di Cignana locality (horizontal dimension ~1m). (**D**) Breccia containing clasts of metagabbro in a largely calcite matrix at the Bracco Unit exposure.

Figure 3: $\delta^{13}C$ and $\delta^{18}O$ for all of carbonate sampled from all textural settings within the metabasalts (data in **Supplementary Table 2**). The lower unfilled box on the right side of the plot illustrates the range of values for finely disseminated calcite in seafloor-altered basalts (from Furnes et al., 2001). The upper unfilled box shows the $\delta^{18}O$ range possible for carbonate veins in variably seafloor-altered basalts (from Alt and Teagle, 2003; Coggan et al., 2010; R. Coggan, pers. comm., 2014). Also included are data for veins and breccia fillings in metabasalt from Catalina Schist from Bebout (1995). The curved line labeled "Rayleigh Trend" is the trend in $\delta^{13}C$ and $\delta^{18}O$ for closed-system decarbonation approximating a Rayleigh process (i.e., generation and loss of fluid without addition of fluid from external sources). The exact curve length (i.e., decrease in $\delta^{13}C$ possible, related to the fraction of C remaining in the Rayleigh calculation) and the trajectory taken depend on the initial modal abundances of the carbonate and silicate phases and the reactions that take place (the latter producing change in mineral modes). Whole-rock $\delta^{18}O$ values for seafloor-altered oceanic crust are as high as +20‰ but most are in the range of +5 to +10‰ (Alt, 2004). The arrow labeled, "Exchange with H_2O-rich Fluid," indicates the $\delta^{18}O$ shifts that carbonate in metabasalts would experience as influenced by exchange with H_2O-rich fluid containing essentially no C.

Figure 4: Carbon and O isotope plots for select localities divided by textural occurrence of carbonates. (**A**) Bracco and Mt. Fignona Units; (**B**) Monviso (Monviso Unit and Lago Supierore Unit); (**C**) Ubaye Unit, France, and (**D**) Zermatt-Saas and Lago di Cignana.

Figure 5: Isotopic compositions of the ophicarbonates (modified from Clerc et al., 2014; data in **Supplementary Table 2**). Shaded grey areas and lightly shaded grey symbols represent values from the literature for ophicalcites from the low-temperature Iberian margin and Galicia bank (Evans and Baltuck, 1988; Milliken and Morgan, 1996; Plas, 1997; Skelton and Valley, 2000), the Alps, Apennines, and Pyrenees (Brotzu et al., 1973; Barbieri et al., 1979; Weissert and Bernoulli, 1984; Barrett and Friedrichsen, 1989; Demeny et al., 2007; Clerc et al., 2014), and from other high-temperature hydrothermal ophicalcites (Lavoie and Cousineau, 1995; Artemyev and Zaykov, 2010; Jedrysek et al., 2000).

Figure 6: Pseudosections calculated with Perple_X for different basalt compositions with *P-T* paths from four modern subduction zones (dashed white lines) from van Keken et al. (2011).

T = Tonga, NV = N. Vanuatu, N = Nankai, and C= Cascadia. Basaltic compositions are from Staudigel et al. (1989), Alt et al. (1996), Staudigel et al. (1996), and King et al. (2004), and are provided in **Supplementary Table 4**. Mineral abbreviations are from Whitney and Evans (2010) with the exception of the combined carbonate phases (Carb). Note the very different starting CO_2 concentrations in these compositions.

Figure 7: Mineral modal abundances calculated with Perple_X for four modern day subduction zones using the average composition of ODP 417/418 (see the pseudosection for this composition in **Fig. 6C**). **A** = Tonga; **B** = N. Vanuatu; **C** = Nankai; **D** = Cascadia.

Figure 8. (**A**) Volatiles isopleth diagram of a composition from ODP 417/418 (Staudigel et al., 1996) containing a relatively high H_2O content. Dashed grey lines represent H_2O content and solid black lines represent the CO_2 content. Solid grey lines display *P-T* paths for four modern day subduction zones (Syracuse et al, 2010; van Keken et al., 2011) and are labeled the same as **Figs. 6C and 7**. Blue boxes represent the *P-T* estimates of the sites sampled in this study. (**B**) Closed-system devolatilization of the average composition from ODP 417/418 (Staudigel et al., 1996) across three modern day subduction zones (Tonga [cool], N. Vanuatu [intermediate], and Cascadia [warm]; see **A**). These *P-T* paths were taken from Syracuse et al. (2010) and van Keken et al. (2011; P. van Keken, personal communication, 2013). Light grey-shaded area represents metabasalts investigated in this study. Dark grey shaded area represents the global average of modern day sub-arc depths

Figure 9: T-X_{CO_2} diagrams from the average basaltic composition of ODP 417/418 (composition from Staudigel et al., 1996; see **Supplementary Table 4**). **Panel A** shows the compositions at 15 kbar and **Panel B** shows compositions at 25 kbar. **Panels 1-2** detail the modal abundance changes that would occur in **Panel A** with the infiltration of an H_2O-rich fluid at two different temperatures. **Panels 3-4** detail the modal abundance changes that would occur in **Panel B** with the infiltration of an H_2O-rich fluid at two different temperatures.

Figure 10: Volatiles isopleth diagram for an ophicarbonate composition (carbonated serpentinite) initially containing 5.5 wt. % CO_2 and 11.0 wt. % H_2O (composition modeled is based on sample G4 in Table 2 of Pelletier et al., 2008). Although such rocks experience significant dehydration over the 550-800˚C temperature range, relatively little CO_2 is lost and even the warmest of the *P-T* paths (Cascadia) results in only ~15% loss. For similar bulk compositions, Kerrick and Connolly (1998) calculated similar near-complete CO_2 retention along the *P-T* gradient of our units (for forearcs), but considerably higher CO_2 losses for the depth interval over which the top of the slab is heating by exposure to the convecting mantle wedge. The C input into subduction zones in this lithology is highly uncertain, with the estimates in **Table 1** indicating contributions of ~4-21 % of the total C inventory.

Figure 1a

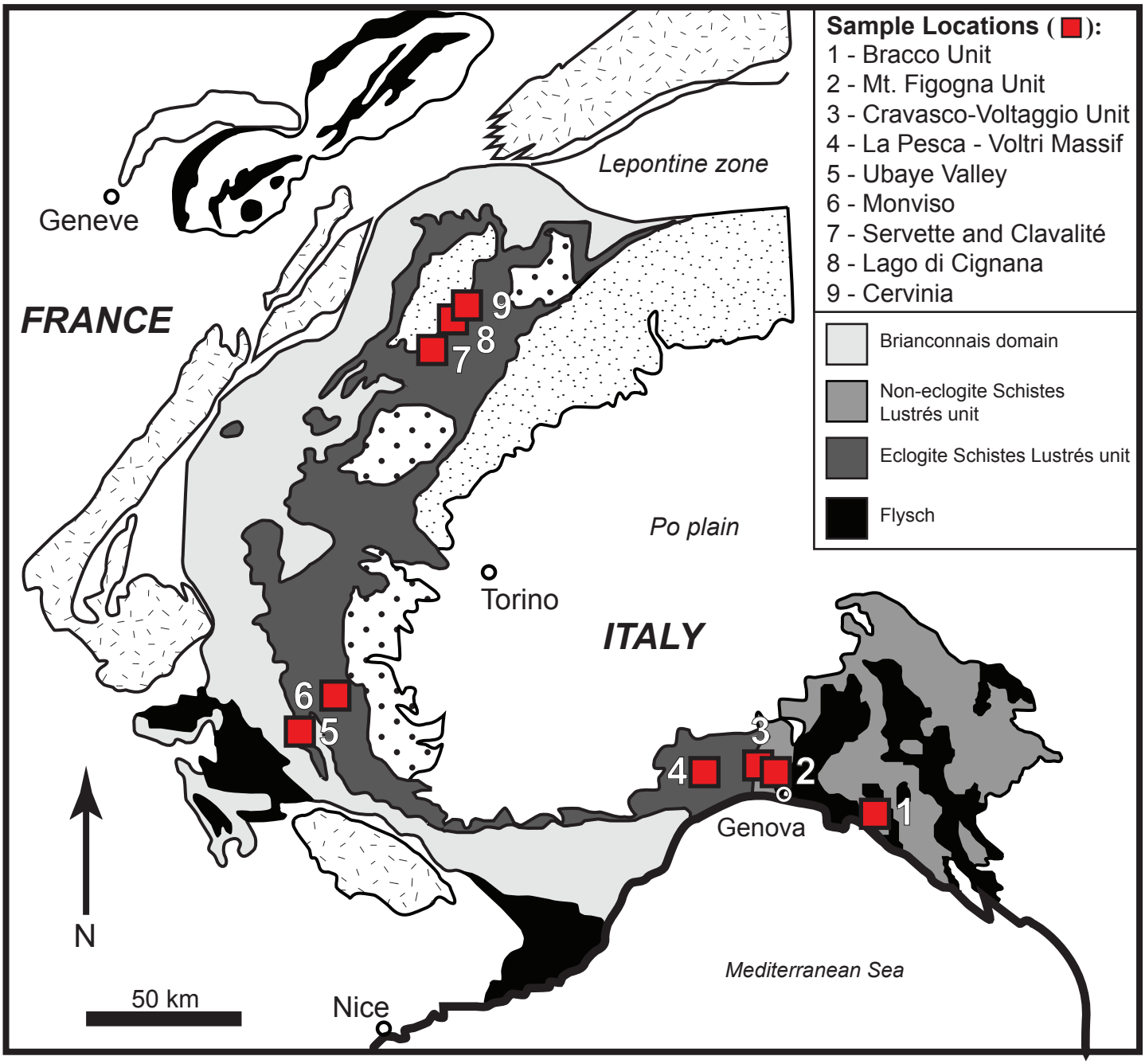
Sample Locations ( ):
1 - Bracco Unit
2 - Mt. Figogna Unit
3 - Cravasco-Voltaggio Unit
4 - La Pesca - Voltri Massif
5 - Ubaye Valley
6 - Monviso
7 - Servette and Clavalité
8 - Lago di Cignana
9 - Cervinia
Brianconnais domain
Non-eclogite Schistes Lustrés unit
Eclogite Schistes Lustrés unit
Flysch
Lepontine zone
Geneve
FRANCE
Po plain
Torino
ITALY
Genova
Mediterranean Sea
Nice
N
50 km

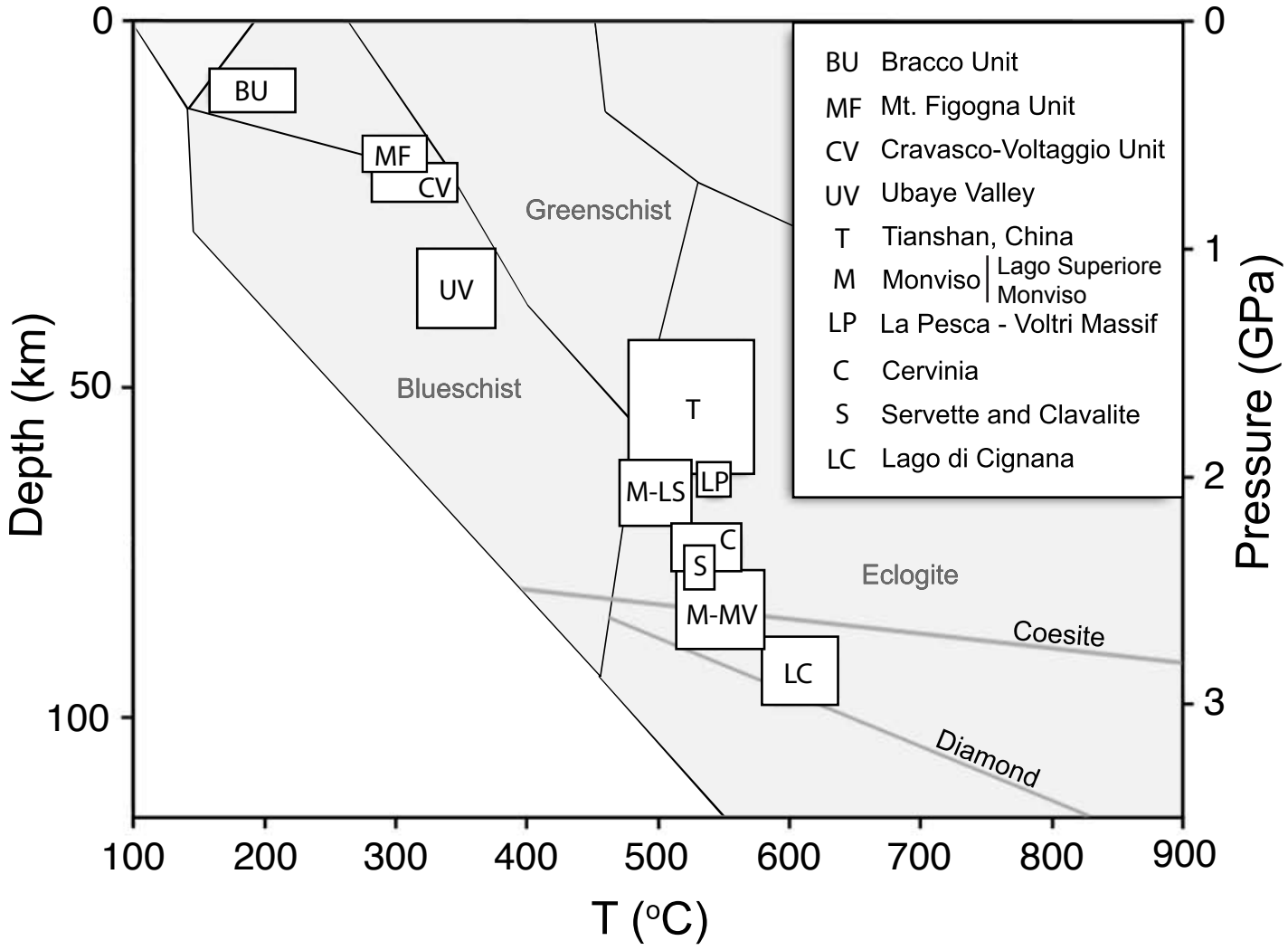
0
50
100
Depth (km)
0
1
2
3
Pressure (GPa)
100
200
300
400
500
600
700
800
900
T (°C)
BU
MF
CV
UV
T
M-LS
LP
C
S
M-MV
LC
Greenschist
Blueschist
Eclogite
Coesite
Diamond
BU Bracco Unit
MF Mt. Figogna Unit
CV Cravasco-Voltaggio Unit
UV Ubaye Valley
T Tianshan, China
M Monviso | Lago Superiore Monviso
LP La Pesca - Voltri Massif
C Cervinia
S Servette and Clavalite
LC Lago di Cignana

Figure 1b

Figure 2

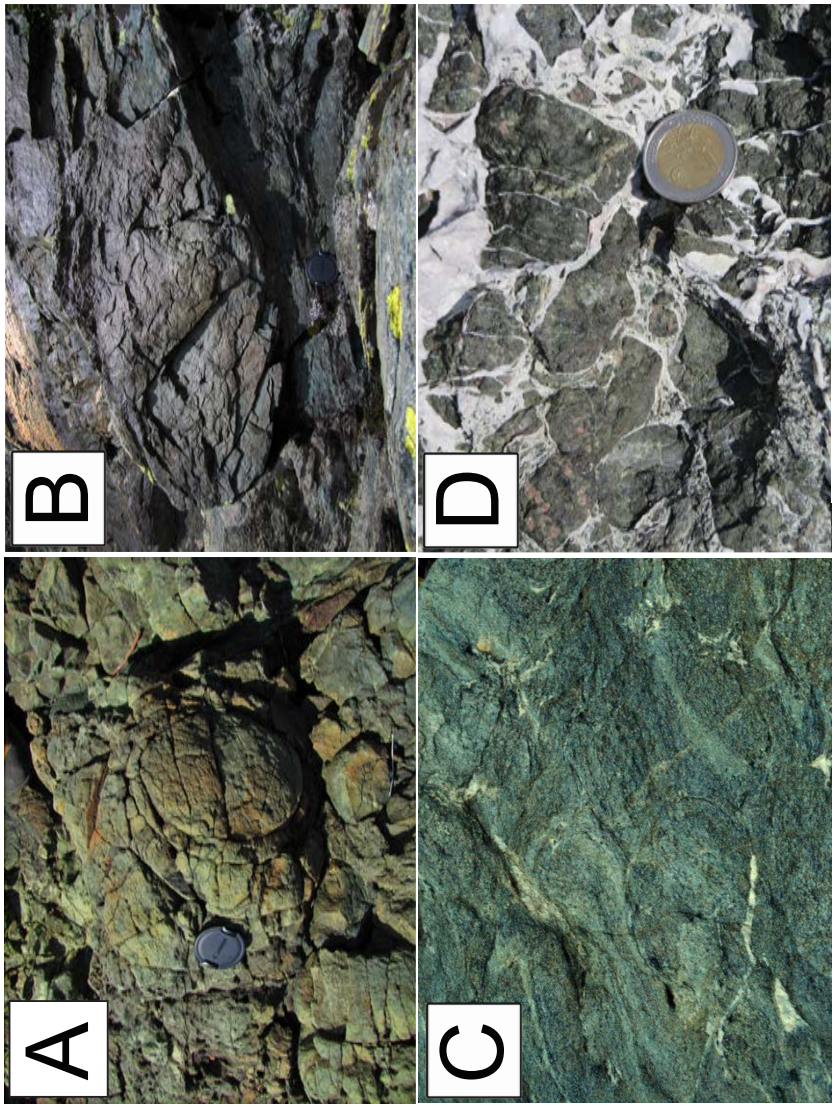

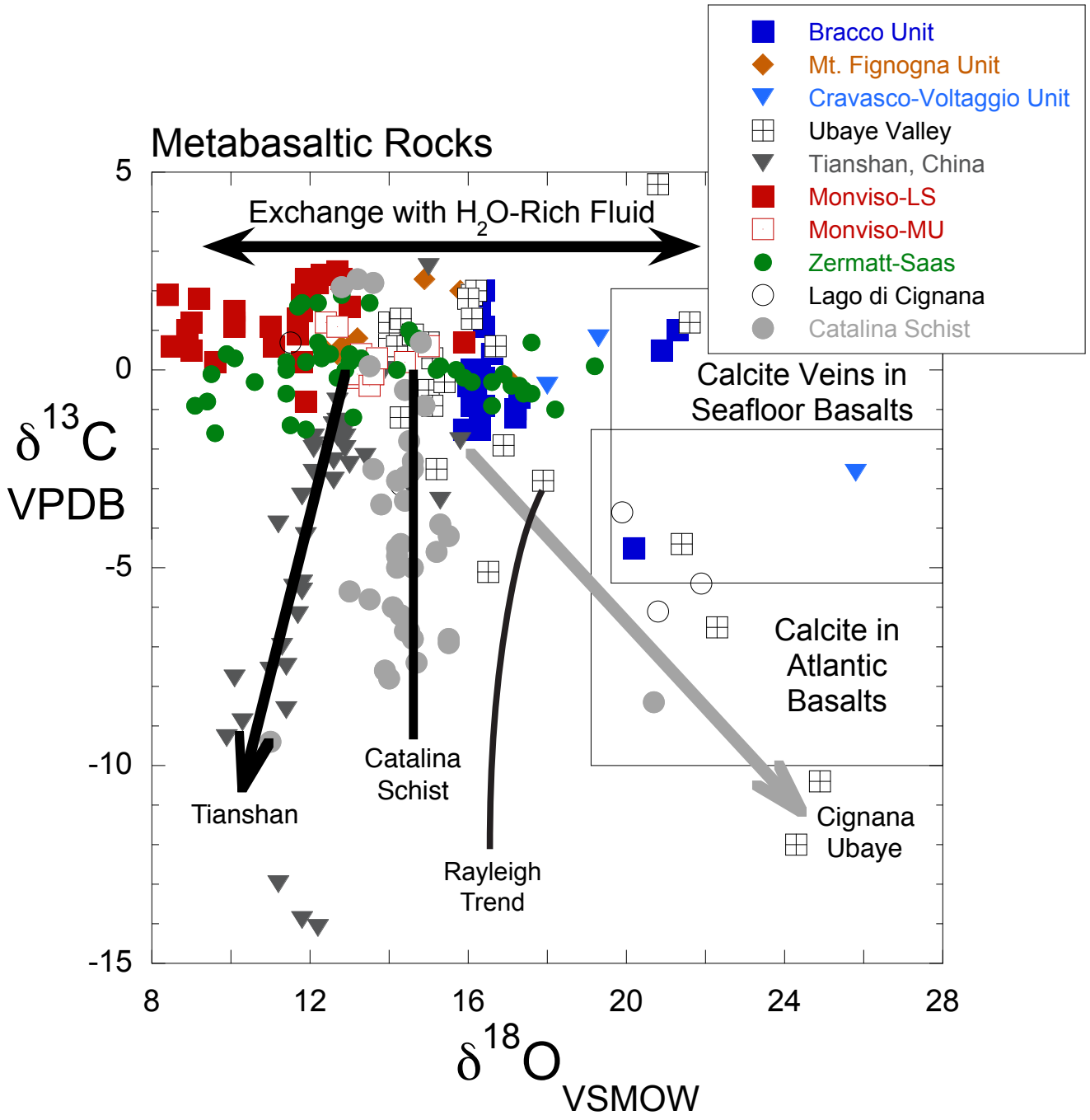
Metabasaltic Rocks
Exchange with H2O-Rich Fluid
Bracco Unit
Mt. Fignogna Unit
Cravasco-Voltaggio Unit
Ubaye Valley
Tianshan, China
Monviso-LS
Monviso-MU
Zermatt-Saas
Lago di Cignana
Catalina Schist
Calcite Veins in Seafloor Basalts
Calcite in Atlantic Basalts
Tianshan
Catalina Schist
Rayleigh Trend
Cignana
Ubaye
δ13C VPDB
δ18O VSMOW
5
0
-5
-10
-15
8
12
16
20
24
28

Figure 3

Figure 4

Figure 4.

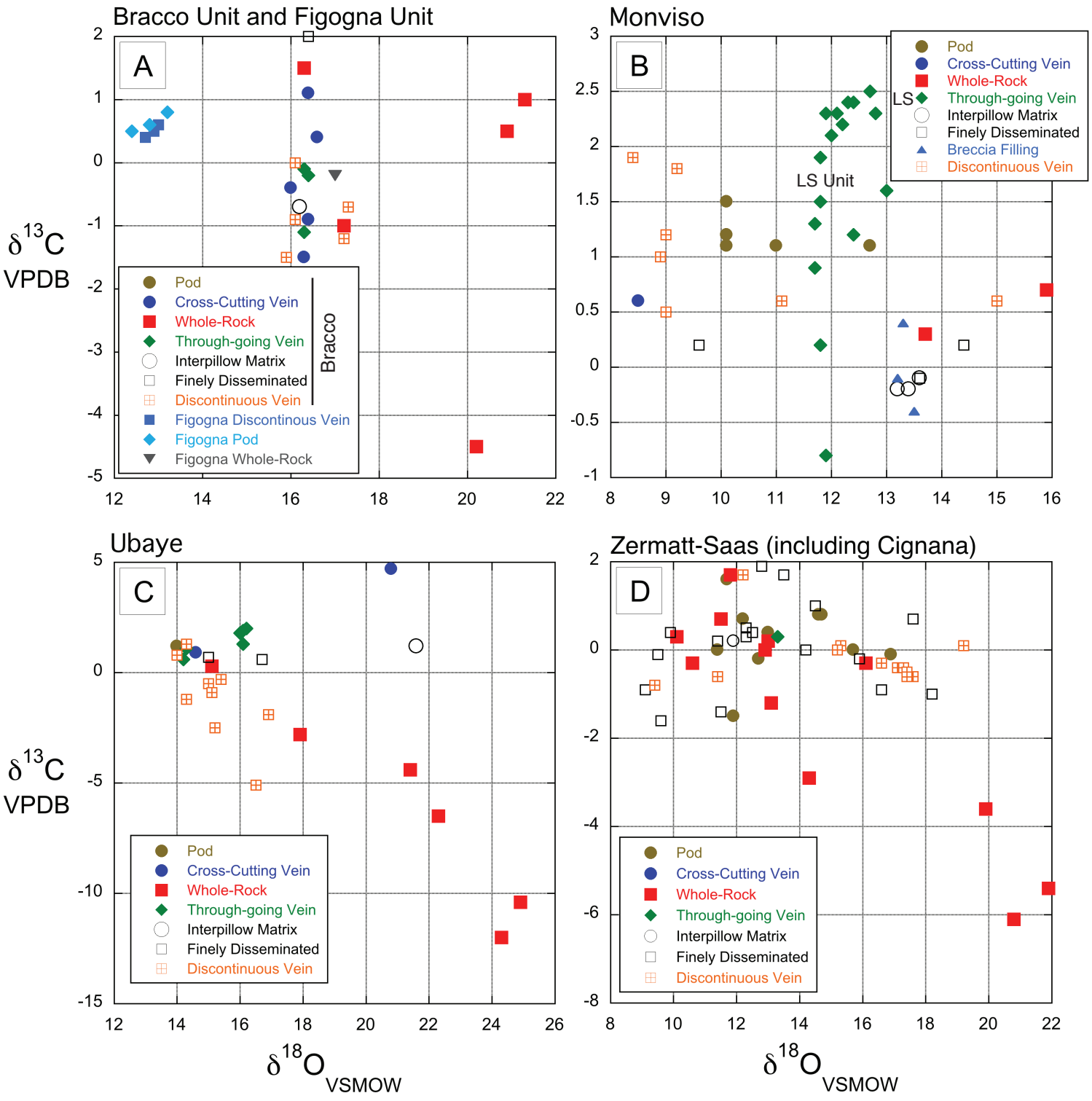

Figure 5

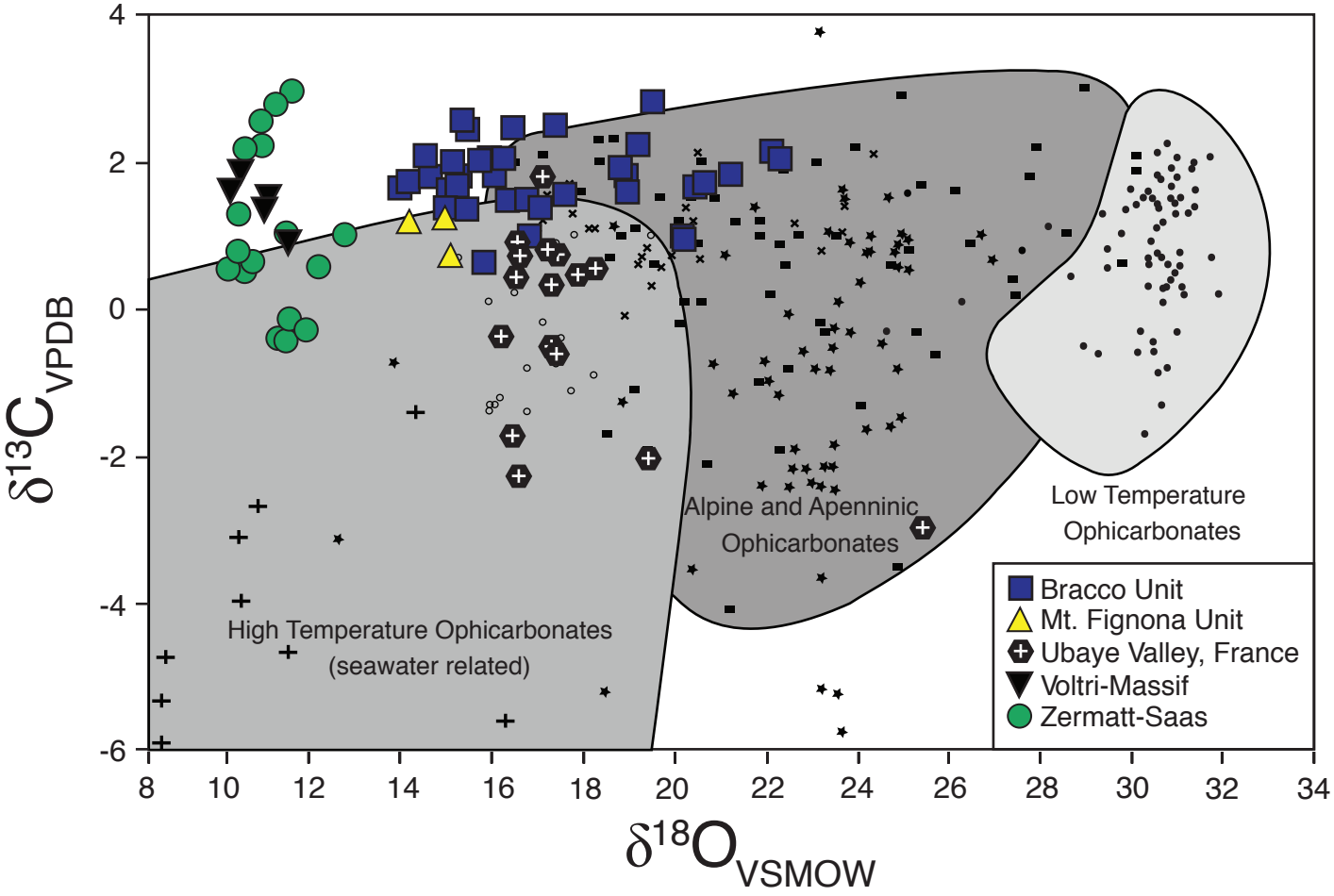

Figure 5

Figures 6 and 7

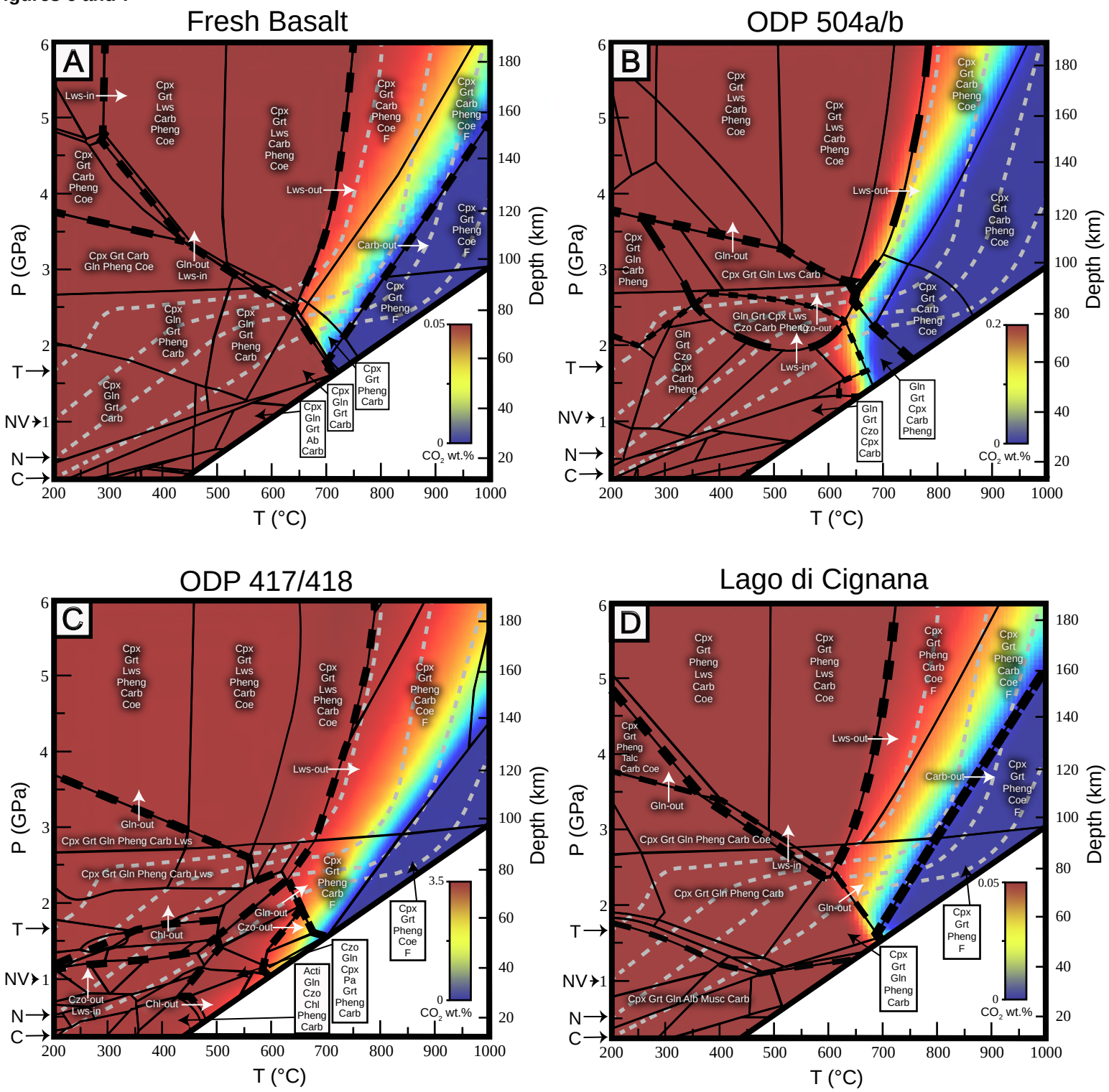

Figure 6

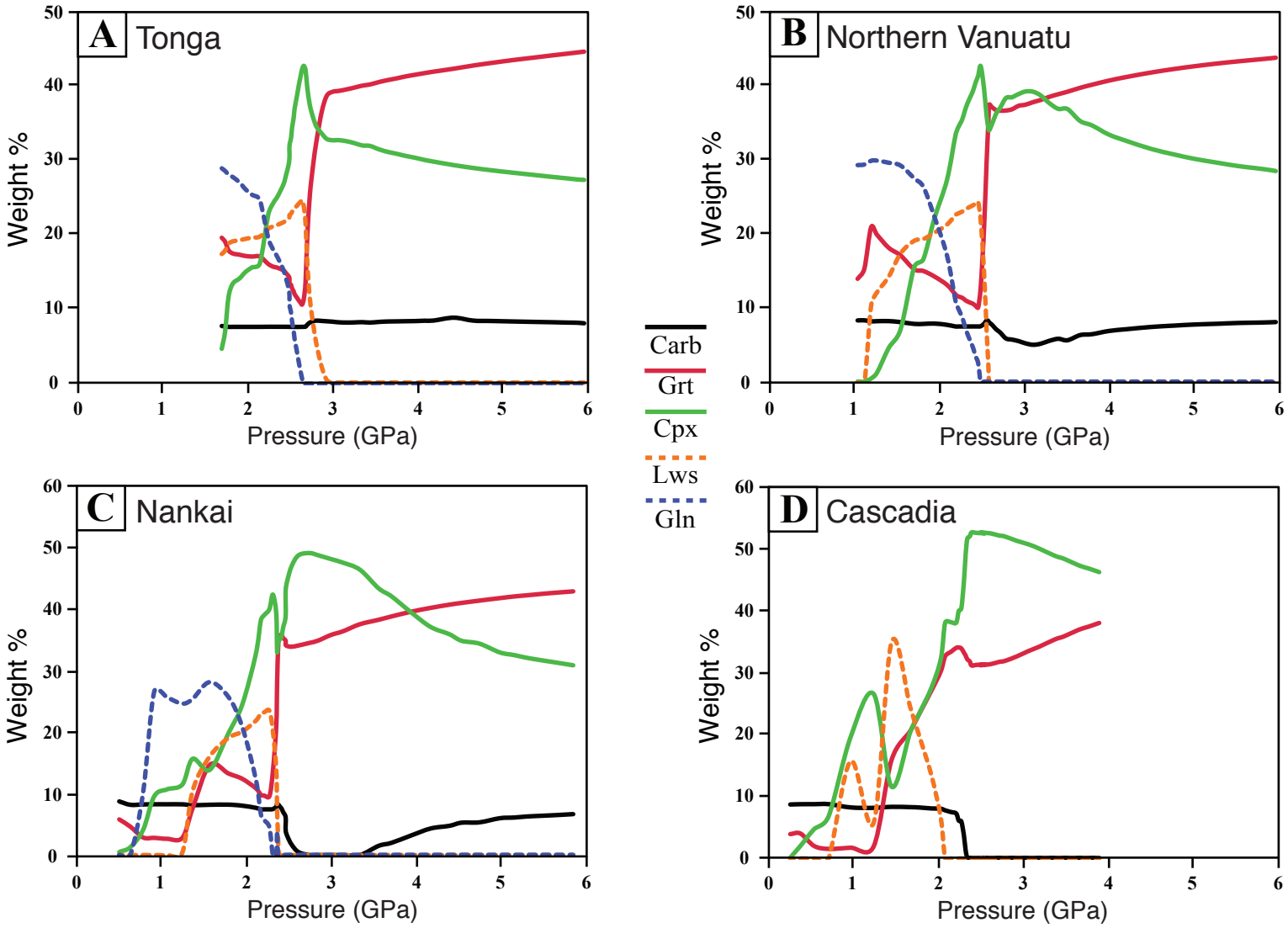
A Tonga
B Northern Vanuatu
C Nankai
D Cascadia
Weight %
Pressure (GPa)
Carb
Grt
Cpx
Lws
Gln

Figure 7

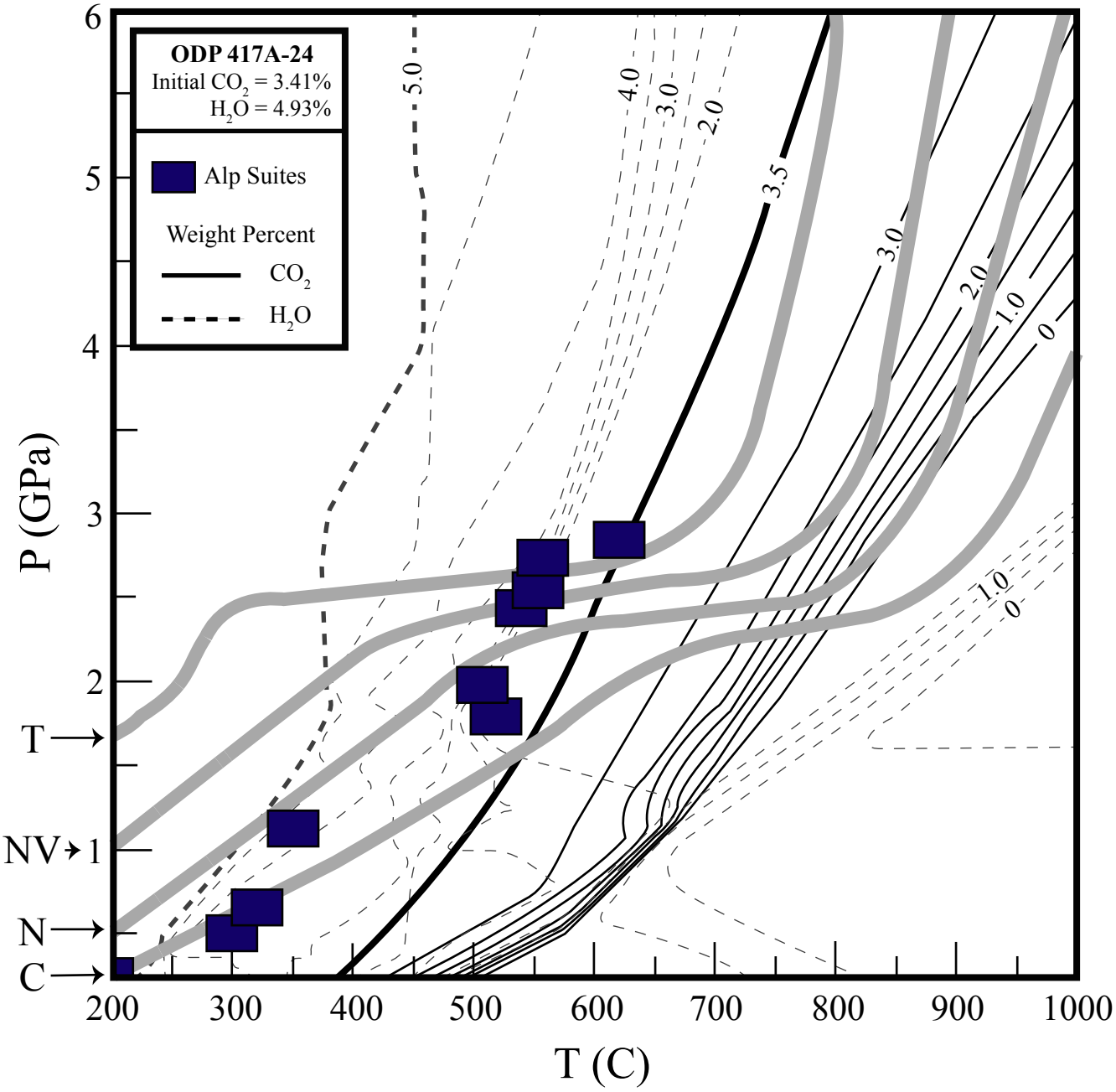
ODP 417A-24
Initial CO_2 = 3.41%
H_2O = 4.93%
Alp Suites
Weight Percent
CO_2
H_2O
5.0
4.0
3.0
2.0
3.5
3.0
2.0
1.0
0
1.0
0
P (GPa)
T
NV
N
C
200
300
400
500
600
700
800
900
1000
T (C)

Figure 8a

Figure 8b and 9

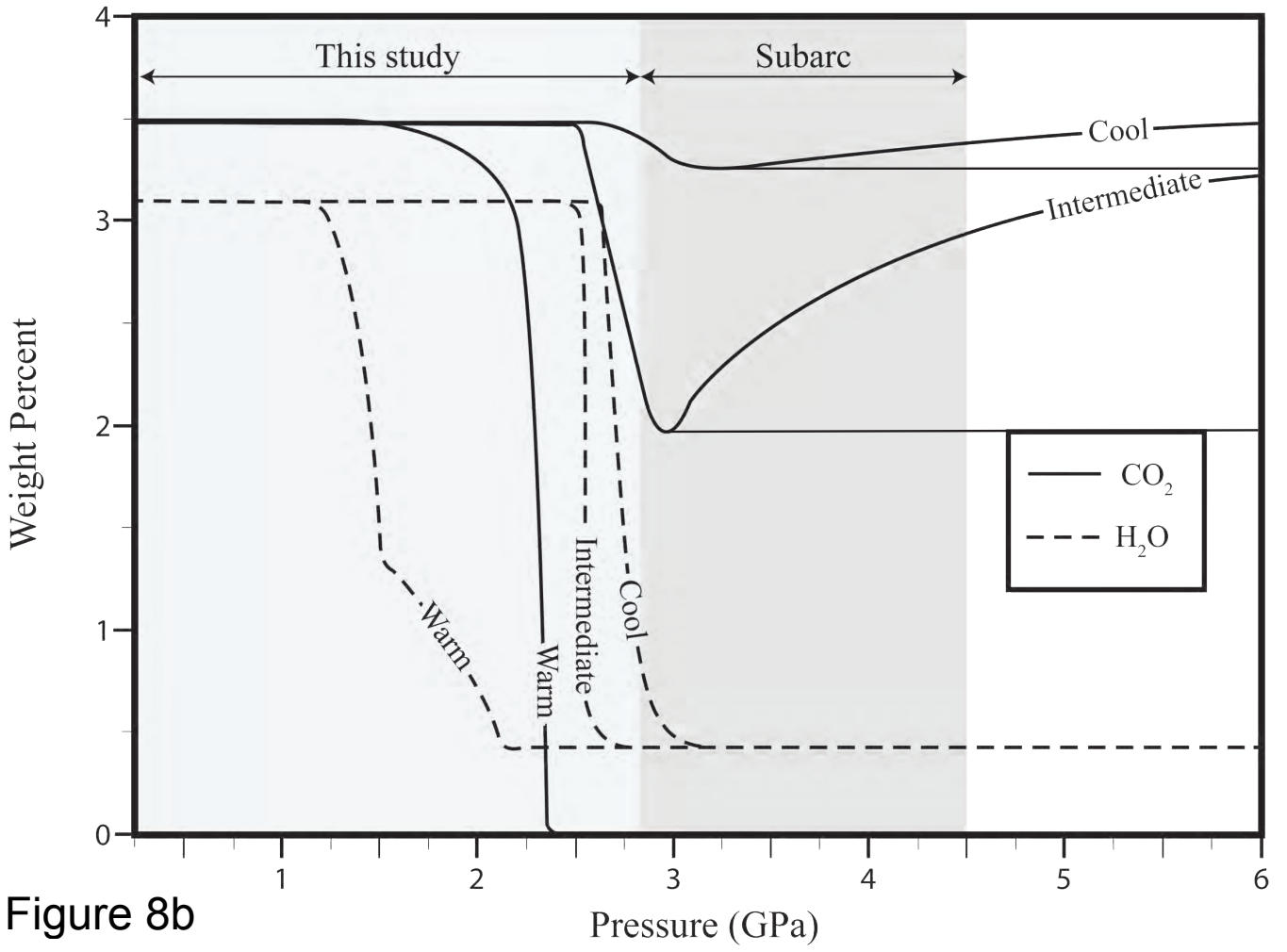

Figure 8b

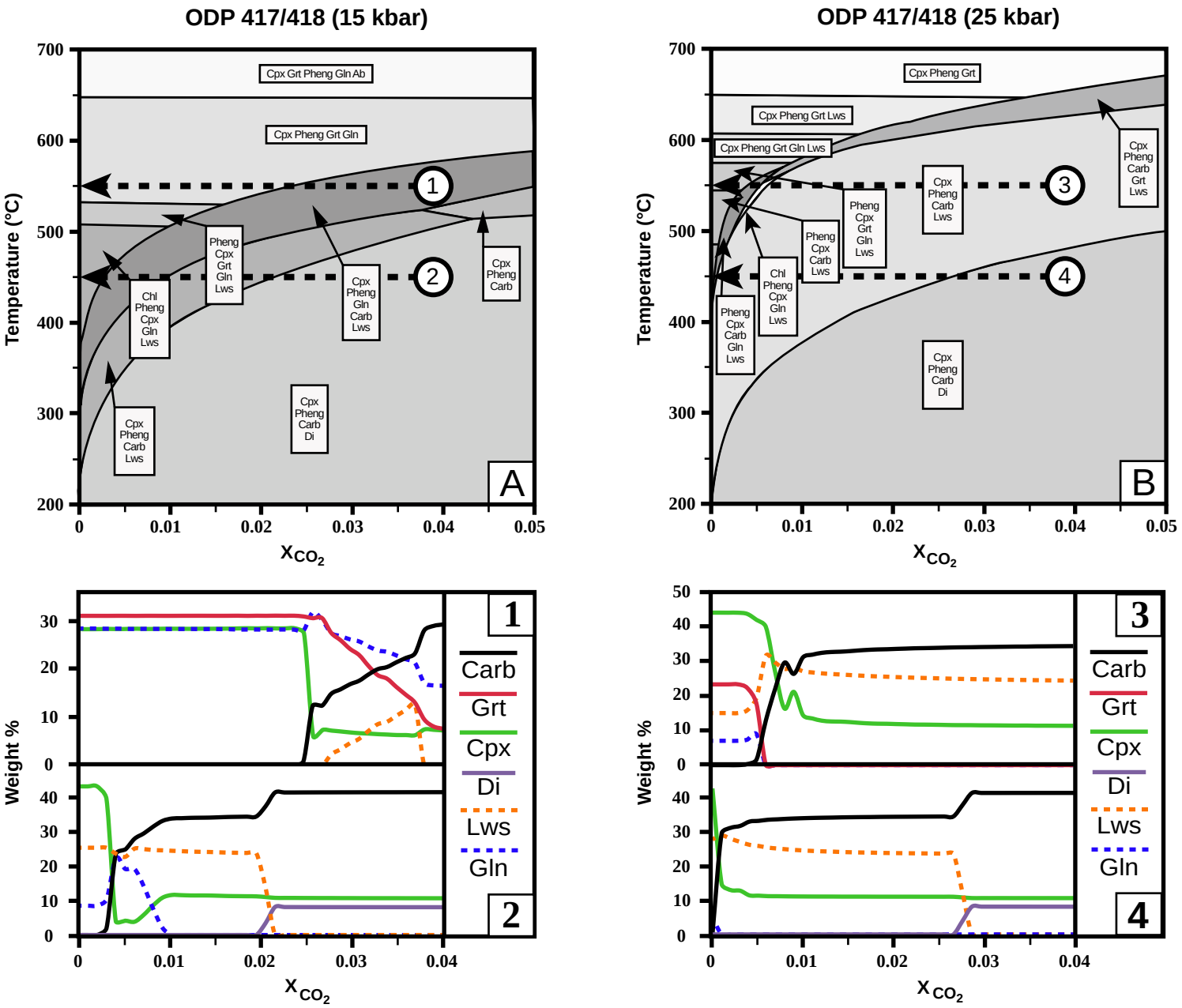
ODP 417/418 (15 kbar)
ODP 417/418 (25 kbar)
Temperature (°C)
X_{CO_2}
Cpx Grt Pheng Gln Ab
Cpx Pheng Grt Gln
Pheng Cpx Grt Gln Lws
Chl Pheng Cpx Gln Lws
Cpx Pheng Gln Carb Lws
Cpx Pheng Carb
Cpx Pheng Carb Lws
Cpx Pheng Carb Di
A
Cpx Pheng Grt
Cpx Pheng Grt Lws
Cpx Pheng Grt Gln Lws
Pheng Cpx Grt Gln Lws
Cpx Pheng Carb Lws
Cpx Pheng Carb Grt Lws
Chl Pheng Cpx Gln Lws
Pheng Cpx Carb Lws
Pheng Cpx Carb Gln Lws
B
Weight %
Carb
Grt
Cpx
Di
Lws
Gln
1
2
3
4

Figure 9

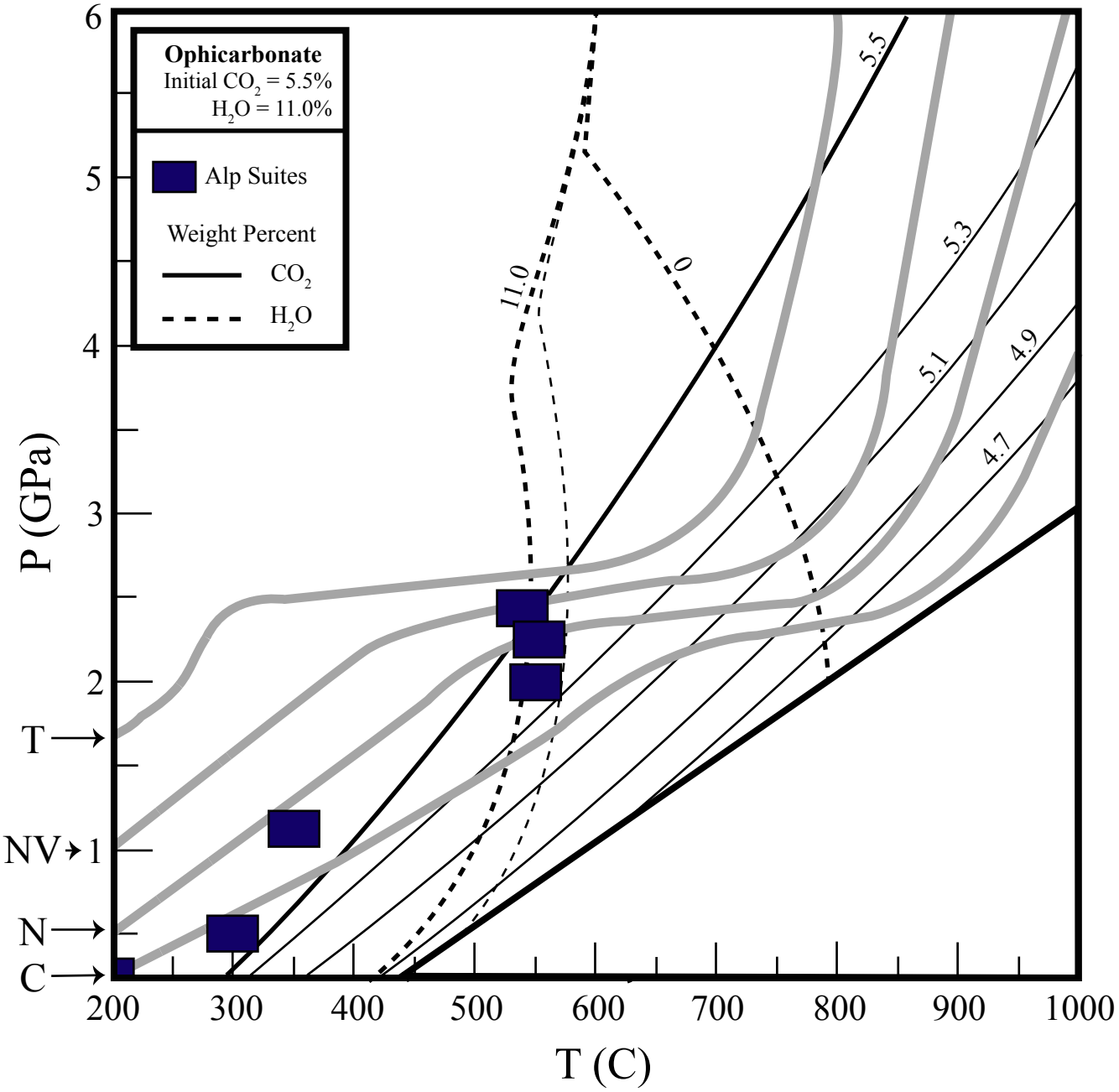
Ophicarbonate
Initial CO_2 = 5.5%
H_2O = 11.0%
Alp Suites
Weight Percent
CO_2
H_2O
11.0
0
5.5
5.3
5.1
4.9
4.7
P (GPa)
T (C)
T
NV
N
C
6
5
4
3
2
1
200
300
400
500
600
700
800
900
1000

Figure 10

Table 1

Click here to download Table: Table1Fluxes92414.pdf

Input (x 10^{12} mol C/yr)				
	Sediments	**Basalts**	**Ultramafics**	**Total**
Bebout (2007, 2014)*	0.9 - 4.8	3.1 - 4.0	*0.4 - 0.8***	*4.4 - 9.6*
Dasgupta (2013)	1.1 - 1.4	3.0 - 5.1	0.4 - 0.8	4.5 - 7.3
Hilton et al. (2002)	1.34	2.12	*0.4 - 0.8***	*3.86 - 4.26*
Jarrard (2003)	1.2	2.27		*3.87 - 4.27*

Output (x 10^{12} mol C/yr)		Return Efficency
	Arc Gas	
Varekamp et al. (1992)	1.5	16 - 80%
Marty & Tolstikhin (1998)	2.5	
Sano & Williams (1996)	3.1	

*The methods for calculating these fluxes are presented in Sadofsky and Bebout (2003).

**from Dasgupta (2013; this flux is added to the sediments and basalts estimates by the other authors)

Table 1. Estimates of C subduction input and output fluxes from the recent literature.

Table 2

Click here to download Table: Table2TexturalSettings92414.pdf

Unit	Location*	Interpillow Material	Outcrop-scale veins	Hand sample scale veins
Bracco Unit	Zerli			
Bracco Unit	Foppo	XX	X	XX
	Porto Pidocchio	XXX	XX	XX
Mt. Figogna Unit	Figogna	XX		X
Mt. Figogna Unit	Pietra Lavezzara	XX		X
Cravasco-Voltaggio Unit	Lencisa	X		
Ubaye Valley, France	Pic du Pelvat	XXX		XX
Lago Superiore Unit	Monviso	X	X	XX
Monviso Unit	Monviso	XX		
Zermatt-Saas Ophiolite	Cervinia	XXX		
Zermatt-Saas Ophiolite	Servette	XX		X
Zermatt-Saas Ophiolite	Clavalite	XX		
Zermatt-Saas Ophiolite	Lago di Cignana			

X - Present XX - XXX - Abundant

Table 2. Textural settings of carbonate at localities for which C and O isotope data are presented in this paper.

Table 3
Click here to download Table: Table3CCyclingCGeol20815.pdf

Table 3. Extents of Loss of CO_2 in 80-120 km Depth Range, Closed-System Models Only (Figs. 8A, 10; Kerrick and Connolly, 2001a)

	Cascadia	Nankai	N. Vanuatu	Tonga
417A-24 (basalt)	100%	100	43	7
Ophicarbonate	15	13	7	3
Sediment Composition (from Plank and Langmuir, 1998)				
GLOSS	100	100	100	29
Antilles	100	100	100	61
Marianas	17	10	7	2
Vanuatu	23	13	6	0

Supplementary Tables 1-4

Click here to download Background dataset for online publication only: MergedSupplTables20815.pdf